

NEW INSIGHTS INTO THE PROBLEM OF THE SURFACE GRAVITY DISTRIBUTION OF COOL DA WHITE DWARFS

P.-E. Tremblay¹, P. Bergeron¹, J. S. Kalirai², and A. Gianninas¹

¹*Département de Physique, Université de Montréal, C.P. 6128, Succ. Centre-Ville, Montréal, QC H3C 3J7, Canada*

²*Space Telescope Science Institute, 3700 San Martin Drive, Baltimore, MD 21218, USA*

tremblay@astro.umontreal.ca, bergeron@astro.umontreal.ca,
jkalirai@stsci.edu, gianninas@astro.umontreal.ca

ABSTRACT

We review at length the longstanding problem in the spectroscopic analysis of cool hydrogen-line (DA) white dwarfs ($T_{\text{eff}} < 13,000$ K) where gravities are significantly higher than those found in hotter DA stars. The first solution that has been proposed for this problem is a mild and systematic helium contamination from convective mixing that would mimic the high gravities. We constrain this scenario by determining the helium abundances in six cool DA white dwarfs using high-resolution spectra from the Keck I 10-m telescope. We obtain no detections, with upper limits as low as $\text{He}/\text{H} = 0.04$ in some cases. This allows us to put this scenario to rest for good. We also extend our model grid to lower temperatures using improved Stark profiles with non-ideal gas effects from Tremblay & Bergeron and find that the gravity distribution of cool objects remains suspiciously high. Finally, we find that photometric masses are, on average, in agreement with expected values, and that the high-log g problem is so far unique to the spectroscopic approach.

Subject headings: white dwarfs — stars: atmospheres — line: profiles

1. ASTROPHYSICAL CONTEXT

The most accurate method for determining the atmospheric parameters of hydrogen-line (DA) white dwarfs — T_{eff} and $\log g$ — is through a detailed comparison of the observed Balmer line profiles with the predictions of model atmospheres. This so-called spectroscopic technique was applied to a sample of 37 cool ($T_{\text{eff}} \lesssim 12,000$ K) DA stars by

Bergeron et al. (1990) who showed that the surface gravities inferred from spectroscopic measurements were significantly larger than the canonical value of $\log g \sim 8$ expected for these stars. This result was readily interpreted as evidence for convective mixing between the thin superficial hydrogen layer with the more massive underlying helium envelope, a process originally, and independently, proposed by Koester (1976), Vauclair & Reisse (1977), and D’Antona & Mazzitelli (1979). In this mixing process, helium brought to the surface would remain spectroscopically invisible because of the low photospheric temperatures. However, the helium abundance can still be determined from a detailed examination of the high Balmer lines, since the presence of helium increases the photospheric pressure, and thus produces a quenching of the upper levels of the hydrogen atom which, in turn, affects the line profiles (Liebert & Wehrse 1983). Bergeron et al. (1991) showed on a more quantitative basis that the effects produced on the hydrogen lines at high $\log g$ — or high masses — could not be distinguished from those produced by the presence of large amounts of helium in the atmospheres of cool DA stars. Such helium-enriched DA white dwarfs would simply *appear* to have high surface gravities when analyzed under the assumption of pure hydrogen atmospheres. By assuming instead a canonical value of $\log g = 8$ for all stars in their sample, Bergeron et al. (1990) were able to demonstrate that the surface compositions of most cool DA white dwarfs are contaminated by large amounts of helium, sometimes as high as $\text{He}/\text{H} \sim 20$.

This astrophysical interpretation, however, rests heavily on the theoretical framework, based on the occupation probability formalism of Hummer & Mihalas (1988), which was implemented by Bergeron et al. (1991) to properly model the hydrogen line profiles. It is thus entirely plausible that these improved model spectra yield large spectroscopic $\log g$ values simply because of inaccuracies in the input physics. With this idea in mind, Bergeron et al. (1992, hereafter BSL92) applied the spectroscopic technique to a large sample of DA white dwarfs that are sufficiently hot ($T_{\text{eff}} \gtrsim 13,000$ K) to avoid any theoretical uncertainties related to the onset of convective energy transport at low effective temperatures, and to the possible presence of spectroscopically invisible traces of helium. The assumptions of radiative atmospheres with pure hydrogen compositions were then perfectly justified. The spectroscopic analysis of BSL92 allowed the first measurement of the $\log g$ and mass distributions of DA stars with an unprecedented accuracy. In particular, the spectroscopic $\log g$ distribution showed a sharp peak with a mean value of 7.909 with a dispersion of only 0.257, in agreement with the expected mean value for DA stars. Hence the spectroscopic technique and model spectra seemed to produce reasonably sound results, at least in this temperature range.

Around the same time, Bergeron et al. (1992) showed that the assumed parametrization of the convective efficiency, treated within the mixing-length theory in white dwarf models,

could affect the emergent fluxes, and in particular the predicted line profiles of DA stars in the range $T_{\text{eff}} \sim 8000 - 14,000$ K. This sensitivity suggests that perhaps the earlier interpretation of the presence of invisible traces of helium in cool DA stars could be caused by an inadequate parametrization of the mixing-length theory. In an attempt to properly calibrate the convective efficiency in the atmospheres of DA stars, Bergeron et al. (1995, hereafter B95) studied a sample of 22 ZZ Ceti stars and showed that the so-called $\text{ML2}/\alpha = 0.6$ version of the mixing-length theory (where α is the mixing-length to pressure scale height ratio) yielded the best internal consistency between optical and UV effective temperatures, trigonometric parallaxes, V magnitudes, and gravitational redshift measurements¹. Yet, despite this adopted calibration, the large $\log g$ values observed in cool DA stars remained.

Our current view of what we will now refer to as the “high- $\log g$ problem” is best summarized in Figure 1, where we show the distribution of surface gravity as a function of effective temperature for the sample of over 1200 relatively bright DA white dwarfs of Gianninas et al. (2009), drawn from the online version of the Villanova White Dwarf Catalog² (see also similar results in Liebert et al. 2005; Bergeron et al. 2007; Kepler et al. 2007; Koester et al. 2009; Gianninas et al. 2009). The model spectra used to determine our atmospheric parameters rely on the improved Stark broadening profiles of Tremblay & Bergeron (2009, hereafter TB09); these models are discussed further in § 3. While the hotter DA stars in Figure 1 follow a distribution close to the canonical mean of $\log g = 8$, the surface gravities are shown to increase suddenly below $T_{\text{eff}} \sim 12,500$ K to a constant average value of $\log g \sim 8.2$. Such high $\log g$ values cannot be real, of course, since white dwarf stars are expected to cool at constant radii. Furthermore, DA white dwarfs at $T_{\text{eff}} \sim 12,500$ K have cooling ages of the order of 1 Gyr or so, and they can hardly represent a distinct galactic population (see additional discussions in Kepler et al. 2007 and Koester et al. 2009). Consequently, inaccuracies in the model atmosphere calculations or inadequate assumptions about the composition of these stars need to be called upon to account for the observed trend. This longstanding problem represents a serious hurdle to obtaining reliable atmospheric parameters at the cool end of the white dwarf evolutionary sequence. This, in turn, may affect our determination of the white dwarf luminosity function (e.g., Harris et al. 2006) and our ability to use white dwarfs as reliable cosmochronometers and distance indicators (Fontaine et al. 2001; Hansen et al. 2007).

Bergeron et al. (2007) and Koester et al. (2009) have produced the most recent and ex-

¹Koester et al. (1994) arrived at a similar conclusion with a somewhat equivalent version of the mixing-length theory, $\text{ML1}/\alpha = 2.0$, although their analysis was based on a single object.

²<http://www.astronomy.villanova.edu/WDCatalog/index.html>

tensive reviews of the high- $\log g$ problem and the possible solutions, but none appear very satisfactory to date. In particular, Koester concludes that inaccuracies in the treatment of convection in model atmospheres is responsible for the problem, for the lack of a better alternative. The mixing-length theory currently used in the models is indeed a crude approximation that makes use of a free parameter, but model spectra properly calibrated yield atmospheric parameters that are quite reasonable, in particular for stars near the ZZ Ceti instability strip (see, e.g., Gianninas et al. 2006). Furthermore, Ludwig et al. (1994) showed with more sophisticated 2D hydrodynamic models that the mixing-length theory was roughly correct to predict the temperature structure of the photospheric regions of DA white dwarfs. More detailed comparisons may prove otherwise, however. Their results do suggest that deeper layers have a significantly higher convective efficiency than predicted from the mixing-length theory, but this has little effect on the predicted spectra.

The solution originally proposed by Bergeron et al. (1990) that the presence of helium in the atmospheres of cool DA stars is responsible for the high- $\log g$ problem cannot be tested directly since helium becomes spectroscopically invisible at the effective temperatures and expected helium-to-hydrogen abundance ratios where the problem manifests itself. Or at least, this used to be our common understanding. This view has recently been challenged by two important discoveries. Koester et al. (2005) were the first to report the detection of weak helium lines in a DA star (HS 0146+1847) with a temperature slightly below $T_{\text{eff}} \sim 13,000$ K; this white dwarf turns out to be a peculiar helium-dominated and metal-rich DAZB star. More importantly, HIRES spectroscopic observations with Keck of the metal-rich DAZ star GD 362 revealed the presence of a very weak He I $\lambda 5877$ absorption feature (Zuckerman et al. 2007), in a white dwarf with an estimated temperature of only $T_{\text{eff}} \sim 10,000$ K. The detailed model atmosphere analysis by Zuckerman et al. also revealed that GD 362 has in fact a helium-dominated atmosphere. Interestingly enough, GD 362 and HS 0146+1847 are also surrounded by a circumstellar disk (Becklin et al. 2005; Farihi et al. 2009). These findings clearly demonstrate that helium can indeed be detected *directly* in this temperature range when observed at sufficiently high signal-to-noise ratio and high dispersion. The weak helium lines detected in both white dwarfs could even be reproduced with model spectra.

In this paper, we provide new insights into the problem of the surface gravity distribution of cool DA white dwarfs by presenting observations of six objects with the High Resolution Echelle Spectrometer (HIRES, Vogt et al. 1994) on the Keck I 10-m telescope and attempt to measure, or constrain, *directly* the helium abundance in the atmosphere of DA white dwarfs.

2. THE PRESENCE OF HELIUM IN COOL DA WHITE DWARFS

2.1. A Reassessment of the Convective Mixing Scenario

As discussed above, the contamination of DA white dwarf atmospheres by trace amounts of helium has been the first and longest running solution to the high- $\log g$ problem. In particular, Bergeron et al. (1991) showed that at low effective temperatures ($T_{\text{eff}} \lesssim 12,000$ K), a high surface gravity DA white dwarf with a pure hydrogen atmosphere would appear identical to a helium-enriched DA star with a normal mass. On the right panels of Figure 2, we illustrate a typical example of this degeneracy for the cool DA star LHS 3254, where the spectroscopic fit with pure hydrogen models ($T_{\text{eff}} = 9370$ K, $\log g = 8.27$) is qualitatively equivalent to the fit with a mixed helium/hydrogen composition of He/H = 1.0 at a comparable temperature ($T_{\text{eff}} = 9300$ K), but with a much lower $\log g$ value of 7.81. On the left panels are shown the corresponding fits to the optical *BVRI* and infrared *JHK* photometry. Here, only the effective temperature and the solid angle $\pi(R/D)^2$ are considered free parameters (R is the radius of the star and D its distance from Earth), while the distance is obtained from the trigonometric parallax measurement. It can be seen that the T_{eff} and $\log g$ values obtained from the photometric solutions are not as sensitive to the assumed helium abundance as the spectroscopic solutions. In the example shown here, the helium abundance has in fact been *adjusted* to ensure that the photometric and spectroscopic $\log g$ values agree. We also note that the photometric and spectroscopic temperatures agree even better when helium is included. Hence, photometric and spectroscopic measurements combined with trigonometric parallaxes can effectively provide, in principle, a unique and self-consistent solution for the atmospheric parameters of cool DA stars, assuming of course that the presence of helium is responsible for the high- $\log g$ problem. Unfortunately, parallax measurements are generally not accurate enough, or even unavailable, and there are many instances where photometric $\log g$ values are already larger than spectroscopic values, even with pure hydrogen models (see Boudreault & Bergeron 2005 and the paragraph below).

With this in mind, it is generally preferable to use a statistical approach to quantify the He/H ratio in cool DA stars. If we assume for instance that the masses of cool DA stars are normal — i.e. the same as for hot DA stars — we can fix the mass and consider the effective temperature and the He/H ratio as free parameters in the spectroscopic fitting technique. The results of this experiment are presented in Figure 3, where we show the helium abundance as a function of T_{eff} for the same sample of cool DA stars used in Figure 1, but with the mass of each star set to $0.649 M_{\odot}$, which corresponds to the mean mass derived by TB09 for the DA stars above $T_{\text{eff}} = 13,000$ K in the Palomar-Green sample. The upper limits at the bottom of the figure correspond to objects for which the spectroscopic masses are already below the mean value adopted here. We can clearly see that there is a

concentration of stars with helium abundances in the range $\text{He}/\text{H} \sim 0.1 - 0.3$. These results suggest that a mild but *systematic* helium contamination could shift the mass distribution to the expected lower value. For a better illustration, we refitted the same sample of cool DA stars with a constant value of $\text{He}/\text{H} = 0.25$ — the average helium abundance in this sample — and plotted the results in Figure 4 together with the pure hydrogen solutions. Hence, with a sudden onset of helium contamination near $T_{\text{eff}} \sim 12,500$ K, we can obtain a stable mass distribution throughout the entire white dwarf temperature regime. It must be stressed that this systematic contamination does not prevent *individual* objects like GD 362 from having much larger helium abundances, or even some stars from having pure hydrogen atmospheres. These objects must be rare, however, since the constant mass distribution achieved in Figure 4 can only be recovered if the vast majority of cool DA stars have a mild helium contamination.

As discussed above, the source of this helium contamination could be most easily explained by convective mixing between the thin hydrogen layer and the deeper and more massive helium envelope. The extent of the hydrogen convection zone is displayed in Figure 5 as a function of effective temperature for a $0.6 M_{\odot}$ DA white dwarf, based on evolutionary models with thick hydrogen layers similar to those described by Fontaine et al. (2001). These calculations show that if the hydrogen envelope is thin enough, the bottom of the hydrogen convection zone may eventually reach the underlying and more massive convective helium layer, resulting in a mixing of the hydrogen and helium layers. This figure also indicates that the effective temperature at which mixing occurs will depend on the thickness of the hydrogen envelope. The thicker the envelope, the lower the mixing temperature; if the hydrogen layer is more massive than $M_{\text{H}}/M_{\text{tot}} \sim 10^{-6}$, mixing will never occur. The simplest physical model that can be used to describe this convective mixing process is to assume that hydrogen and helium are homogeneously mixed. Since the helium convection zone is much more massive ($M_{\text{He-conv}}/M_{\text{tot}} \sim 10^{-6}$) than the hydrogen layer when mixing occurs, it is generally assumed that a DA star would be transformed into a helium-atmosphere non-DA white dwarf with only a trace abundance of hydrogen. By performing a statistical analysis of the ratio of hydrogen- versus helium-rich white dwarfs as a function of T_{eff} , Tremblay & Bergeron (2008) demonstrated that such mixing does indeed occur, but not until white dwarfs reach temperatures below ~ 9000 K. Even then, mixing seems to occur for only 15% of all DA stars. This view is consistent with our current understanding that most DA stars probably have thick hydrogen layers with $M_{\text{H}}/M_{\text{tot}} \gtrsim 10^{-6}$ (see Table 7 of Fontaine & Brassard 2008).

Since the helium abundances inferred from Figure 3 are significantly lower than those expected from this standard convective mixing scenario, it is necessary to invoke an alternative and incomplete mixing process that would systematically contaminate the atmospheres of DA stars with only small amounts of helium, perhaps through overshooting. However, the

hydrogen convection zone in a 12,000 K DA white dwarf is very thin according to Figure 5, much smaller than the $\sim 10^{-6} M_{\odot}$ or so expected for the total hydrogen layer mass of most DA stars, and any type of convective overshooting thus appears improbable. If we were to confirm such an incomplete mixing scenario, we would have to review our assumption that hydrogen and helium are homogeneously mixed when convection zones connect, as well as our estimates of the thickness of the hydrogen layers in DA stars.

2.2. Direct Detection of Helium in Cool DA White Dwarfs

According to the incomplete convective mixing scenario, a systematic helium contamination estimated at $\text{He}/\text{H} = 0.25$ (see Fig. 3) would be able to explain the high- $\log g$ problem. Obviously, the actual ratio may vary from star to star, but on average, the helium abundance of individual DA stars must be close to this value if this interpretation is correct. In this section, we attempt to test this scenario through direct observations of helium in the photospheres of cool DA stars. For this purpose, we used our model atmospheres to predict the strength of the He I $\lambda 5877$ line for a wide range of atmospheric parameters. These are similar to those described in TB09, with the exception that we now include the detailed helium line opacity calculations of Beauchamp et al. (1996, and references therein) and Beauchamp et al. (1997), which also take into account the Hummer-Mihalas occupation probability formalism (more details are provided in § 3). In line with the results for GD 362 and HS 0146+1847, we find that helium can indeed be detected spectroscopically in the range of temperatures where the incomplete mixing scenario is believed to occur, but the detection of this helium line requires high-resolution ($R \sim 20,000$) and high signal-to-noise ($S/N \gtrsim 100$) spectroscopic observations. Since the brightest white dwarfs in this temperature range have $V \sim 12.5 - 15.0$, an echelle spectrograph on an 8-meter class telescope is absolutely necessary to detect this weak absorption feature.

With these predictions in hand, we requested one night of observing time on the Keck I 10-m telescope on Mauna Kea with HIRES. Our objective was to observe the spectral region around the He I $\lambda 5877$ line for at least five DA stars with $T_{\text{eff}} < 12,500$ K to investigate whether the helium contamination is indeed systematic. We first computed the S/N and integration time required to achieve a 3σ detection for DA stars selected from the sample of Gianninas et al. (2009). We found that stars below $T_{\text{eff}} \sim 10,500$ K would require more than five hours of observation time to achieve our detection threshold, even for the brightest stars, compromising our original strategy. We thus reduced our target list to a representative sample of six bright DA stars in the range $12,500 \gtrsim T_{\text{eff}} \gtrsim 10,500$ K. The atmospheric parameters for all six white dwarfs are given in Table 1; these are obtained by fitting lower

resolution spectra taken from the spectroscopic survey of Gianninas et al. (2009) with pure hydrogen model atmospheres. The location of these objects in Figure 1 (circles) indicates that they occupy a region in T_{eff} and $\log g$ where the spectroscopic $\log g$ values rise significantly. We note that four DA stars in our sample have surface gravities significantly in excess of the canonical value of $\log g = 8$. Our coolest target, G67-23 (labeled in Fig. 3), is predicted to be a very massive ($M \sim 1.14 M_{\odot}$) white dwarf under the assumption of a pure hydrogen composition. Not surprisingly, five out of six objects also turn out to be ZZ Ceti pulsators.

High S/N spectroscopic observations for all stars in Table 1 were secured on 2009, August 26 using the HIRES instrument with the red collimator and the 0."86 slit ($R \sim 50,000$). The spectroscopic data were reduced using the MAKEE reduction software (version 5.2.4) and carefully calibrated to vacuum wavelengths. We show in Figure 6 the high-resolution spectra for the six stars in the region of the He I $\lambda 5877$ line, along with the predicted helium line profiles. The thick solid lines correspond to the predictions with a systematic helium contamination of $\text{He}/\text{H} = 0.25$, while the dotted lines assume a $0.649 M_{\odot}$ stellar mass. This last assumption implies that any surface gravity measurement above $\log g \sim 8.08$ is attributed to the presence of helium; this applies to only four stars in Table 1 and in Figure 6. *Our results clearly indicate a non-detection of helium for all objects in our sample.*

Our spectroscopic data can provide upper limits on the helium abundance in the photosphere of these stars. We first obtain from our low-resolution spectra the best fitted parameters T_{eff} and $\log g$ for a given helium abundance. We then increase the helium abundance until the depth of the predicted He I $\lambda 5877$ line profile is 3σ above the noise level of our HIRES data³. These upper limits on the helium abundance are reported in Table 1 for each star. For five objects, we find very low upper limits for the He/H abundance ratio (less than one tenth). We must therefore conclude that a mild and systematic helium contamination in the atmospheres of cool DA white dwarfs cannot be the origin of the high- $\log g$ problem.

The case of G67-23 (2246+223) is particularly of interest since our low-resolution optical spectrum exhibits high Balmer lines characteristics of a massive DA star (see Fig. 1b of Lajoie & Bergeron 2007), or alternatively, of a normal mass white dwarf with a helium-dominated atmosphere, such as GD 362. According to Figure 6, however, our observations can rule out this last possibility, although our limit on the helium abundance in this star is not as stringent as for the other five objects in our sample. Finally, we note that another

³Since we oversample the predicted line profiles with the 0.1 \AA resolution, we binned by a factor of 4 to provide better, but still conservative upper limits.

target, G29-38, is a peculiar DAZ star with a circumstellar disk. The detection of helium in this star would have been problematic since the source of the contamination could have been non-stellar. However, our non-detection implies that this object can effectively be used to constrain the incomplete mixing scenario.

We thus demonstrated for the first time that there is probably little to no helium in the photospheres of most cool DA white dwarfs. We believe our results put to rest the scenario invoking an incomplete convective mixing between the hydrogen atmosphere and the underlying helium envelope, and alternative explanations must be sought to solve the high- $\log g$ problem in cool DA stars.

2.3. Helium Contamination in GD 362

For completeness and internal consistency, we reanalyze in this section the available data for GD 362. This object represents the coolest DA star with a direct detection of the He I $\lambda 5877$ line. We reproduce in Figure 7 the observations of GD 362 from Zuckerman et al. (2007) taken from the Keck Observatory Archive (KOA)⁴. We combine in our analysis this HIRES spectrum with the lower resolution optical spectrum of Gianninas et al. (2004) to determine the atmospheric parameters (T_{eff} , $\log g$, and He/H). The general fitting procedure is described in Liebert et al. (2005), although here we only use the lines from H β to H δ in the fit because the higher Balmer lines are heavily contaminated by metallic lines.

Our determination of the helium abundance in GD 362 proceeds in the same way as in Zuckerman et al. (2007). The degeneracy between the He/H abundance ratio and $\log g$ allows us to compute a sequence of best fitting models from the Balmer line analysis, with a set of parameters (T_{eff} and $\log g$) assigned to each helium abundance. The optimal He/H abundance ratio, and the corresponding T_{eff} and $\log g$ values, are then found by fitting the equivalent width of the He I $\lambda 5877$ line profile. Our best fitted parameters for GD 362 are given in Figure 7 together with our prediction of the helium line profile. While the overall strength of the absorption feature is well reproduced, the line core is not predicted as sharp and deep, a discrepancy similar to that reported by Zuckerman et al. (2007, see their Fig. 1). Our value for the effective temperature, $T_{\text{eff}} = 10,560$ K is in excellent agreement with that of Zuckerman et al. (2007, $T_{\text{eff}} = 10,540 \pm 200$ K), although both our $\log g$ and helium abundance determinations differ, within the uncertainties, from the values obtained by Zuckerman et al. (2007), $\log g = 8.24 \pm 0.04$ and $\log \text{He/H} = 1.14 \pm 0.1$ (our internal errors are comparable to those of Zuckerman et al.). The solution obtained by Zuckerman et

⁴www2.keck.hawaii.edu/inst/hires/

al. is actually a poor match to our low-resolution spectrum, although the predicted helium line strength agrees with the HIRES observations. Hence the mass we derive for GD 362, $M = 0.64 M_{\odot}$ (using evolutionary models with thin hydrogen layers), is actually quite average (Zuckerman et al. obtained $0.73 M_{\odot}$). The independent mass determination reported by Kilic et al. (2008), $M = 0.74 M_{\odot}$, which is based on a measurement of the trigonometric parallax of GD 362, actually favors the solution of Zuckerman et al., but see our discussion below.

Since the overall procedures are similar, some of the differences between our results and those of Zuckerman et al. might be attributed to our particular analysis of the higher Balmer lines, or to the treatment of the non-ideal effects in the Hummer-Mihalas occupation probability formalism. In any case, these atmospheric parameter determinations must be taken with caution. First of all, the strength of the hydrogen lines at such high helium abundances is particularly sensitive to the Hummer-Mihalas occupation probability for neutral particles (Koester et al. 2005), and a slight change in the hard sphere radius used in the description of the neutral particle interaction may result in significantly different atmospheric parameters. The current parameterization (see § 5.1) is uncertain in this high-density regime and one could adjust the theory until there is match between our spectroscopic solution and the constraints obtained from the trigonometric parallax measurement of Kilic et al. (2008). Gianninas et al. (2004) also showed that the presence of metals does not affect significantly the atmospheric structure of GD 362 for pure-hydrogen atmospheres, but this assumption has not been fully tested for helium-rich compositions. And finally, as mentioned above, the sharp core of the helium line is not well reproduced by the models, a feature that is not observed in the slightly hotter white dwarf HS 0146+1847. Perhaps hydrogen is not homogeneously distributed in the atmosphere of GD 362, especially if hydrogen is being accreted (Jura et al. 2009).

Despite the preceding discussion, it is clear that GD 362, which was interpreted by Gianninas et al. (2004) as a massive ($M \sim 1.24 M_{\odot}$) white dwarf with a hydrogen-dominated and metal-rich atmospheric composition, is in fact a more average mass white dwarf with a helium-dominated atmosphere. According to the helium abundances inferred in cool DA stars and displayed in Figure 3, such objects must be rare since there are very few stars in the upper part of this diagram. GD 362 (labeled in Fig. 3) is actually the object with the largest helium abundance according to our statistical analysis. Also labeled in this figure is one of our targets, G67-23 (2246+223), which does not show any trace of helium (see Fig. 6). The peculiar helium-dominated star HS 0146+1847, the hotter counterpart of GD 362, was discovered in the SPY sample containing more than ~ 1800 high-resolution spectra; Koester et al. (2009) searched this sample for DA stars with traces of helium, including a fairly large number with temperatures below 13,000 K. The search was also negative,

but with a much larger detection limit than provided here with our Keck I observations. Nevertheless, it is an additional argument that such objects must be very rare.

The existence of the peculiar atmospheric compositions of GD 362 and HS 0146+1847 may be explained by two different scenarios. We may be witnessing white dwarfs in the process of being convectively mixed, a process believed to occur in cooler white dwarfs (Tremblay & Bergeron 2008). This would imply, however, unusually thin hydrogen layers according to the results shown in Figure 5. Alternatively, the mixed H/He composition could have a non-stellar origin, perhaps related to the collision with a water-rich asteroid in the case of GD 362 (Jura et al. 2009), resulting in the accretion of hydrogen onto a helium-rich atmosphere. The fact that these two objects are metal-rich with circumstellar disks suggests that the latter is the most likely explanation until we discover more similar objects.

3. MODEL ATMOSPHERES WITH IMPROVED STARK PROFILES

As discussed in the introduction, our approach with respect to the spectroscopic technique has always been to start with the simplest white dwarf atmospheres to validate the method. For instance, BSL92 demonstrated that the spectroscopic technique is the most accurate method for determining the atmospheric parameters of DA stars using a sample of pure hydrogen atmosphere white dwarfs where convective energy transport can be neglected ($T_{\text{eff}} > 13,000$ K). B95 later extended this spectroscopic analysis to ZZ Ceti stars, which are located in the temperature range where the atmospheric structures are the most sensitive to the assumed convective efficiency. They found in particular that the $ML2/\alpha = 0.6$ parameterization of the mixing length theory (MLT) provided the best internal consistency between optical and UV temperatures. However, this calibration of the convective efficiency in DA stars did not change the persisting problem that higher than average masses were found at low effective temperatures. More recently, TB09 published Stark broadening profiles with the first consistent implementation of the Hummer-Mihalas equation of state. They included non-ideal perturbations from protons and electrons directly inside the Vidal et al. (1970) unified theory of Stark broadening. As a first step, they revisited the BSL92 temperature regime with improved model atmospheres of hot DA stars. They showed convincingly that these models were adequate to describe the observations, resulting also in T_{eff} and $\log g$ measurements significantly larger than those obtained from previous models. In this section, we explore the implications of these improved models on the spectroscopic analysis of cooler DA white dwarfs, including the ZZ Ceti stars.

Following our approach with the spectroscopic technique, we must first recalibrate the convective efficiency using the same approach as B95. The tightest constraint comes from the

comparison of effective temperatures measured independently from optical and UV spectra (see B95 for details). Other constraints, such as trigonometric parallaxes and gravitational redshifts, are not used for this calibration; they will be compared to our models in § 4. We use an improved set of *HST* and *IUE* near-UV observations (Holberg et al. 2003), some of which were not available at the time of the B95 study. We first fit the optical spectra to find T_{eff} and $\log g$ values. In the case of the near-UV spectra, solutions are degenerate in T_{eff} and $\log g$ and both atmospheric parameters cannot be fitted simultaneously. Therefore, we fit the UV spectra by forcing the spectroscopic value of $\log g$, and the parameter α is then varied until an internal consistency is achieved between UV and optical temperatures. Figure 8 (which is an updated version of Figure 11 of B95) indicates that the $\text{ML2}/\alpha = 0.8$ version of the MLT provides the best overall internal consistency. This is a significantly more efficient version of the MLT than estimated by B95 ($\alpha = 0.6$), in closer agreement with that required by nonadiabatic models ($\alpha = 1.0$) to match the empirical blue edge of the ZZ ceti instability strip (see Fig. 9 of Fontaine & Brassard 2008).

We have then computed extensive grids of models down to $T_{\text{eff}} = 1500$ K that connect with the grids used in TB09 at $T_{\text{eff}} = 12,000$ K. Our model grid is calculated with temperature steps of 500 K, and $\log g$ values from 6.5 to 9.5 with steps of 0.5 dex (with two additional grid points at 7.75 and 8.25). We use the improved Stark profiles of TB09 and the updated mixing-length parameter, as discussed above. Since we are mostly interested here in investigating the influence of our improved profiles on the high- $\log g$ problem, we also computed a second grid similar to that used by the Montreal group for the past ten years. These models rely on the Stark profiles of Lemke (1997) with the value of the critical field β_{crit} in the Hummer-Mihalas formalism multiplied by a factor of 2; a more detailed discussion of this ad hoc parameter is provided in TB09. The mass distributions for the cool DA white dwarfs in the sample of Gianninas et al. (2009) are displayed in Figure 9 for both sets of model spectra. These results clearly indicate that our improved line profiles do not help in any way to solve the long lasting problem that the mean spectroscopic mass increases significantly below $T_{\text{eff}} \sim 12,500$ K. However, there is a significant improvement in the range $30,000 > T_{\text{eff}} > 12,500$ K, where the mass distribution appears more constant, in contrast with our previous results where the mean mass slightly decreases at lower temperatures, leading to an unexpected dip in the distribution near $T_{\text{eff}} \sim 13,000$ K (see also Fig. 3 of Gianninas et al. 2009, for a more obvious illustration of this problem). With our improved models, we can now observe a more stable mass distribution down to $T_{\text{eff}} \sim 12,500$ K, followed by a sudden increase in the mean mass below this temperature.

It has been previously suggested that uncertainties in the treatment of the Stark profiles combined with that of the pseudocontinuum opacity originating from the dissolved atomic levels within the occupation probability formalism of Hummer-Mihalas, and in par-

ticular the ad hoc parameterization of β_{crit} , could be responsible for the high- $\log g$ problem (Koester et al. 2009). Our results presented in Figure 9 show that this is likely not the case. The unified theory of Stark broadening from Vidal et al. (1970) still suffers from some approximations, but it would be surprising that additional corrections, such as second order effects, would change the masses by more than 1%. Moreover, the sudden increase in the average mass of DA stars below $\sim 12,500$ K can hardly be explained by a change in Stark profiles since these have a fairly smooth temperature-dependence in this regime.

We finish this section by presenting additional evidence that inaccuracies in the physics included in the model atmospheres are at the heart of the high- $\log g$ problem. We first refer the reader to Figure 2 of TB09, which depicts the effect of including additional lines in the fitting procedure on the measurement of the atmospheric parameters. The top panel shows how both T_{eff} and $\log g$ *decrease* as more lines are considered in the fit. This problem has been discussed at length by Bergeron (1993) who proposed to multiply by a factor of 2 the value of the critical field, β_{crit} , to partially overcome this discrepancy (see middle panel of Fig. 2 of TB09). By including the Hummer-Mihalas formalism directly into the line profile calculations, TB09 managed not only to get rid of this ad hoc factor, but achieved an even better internal consistency between the various Balmer lines (bottom panel of Fig. 2 of TB09). We show in Figure 10 a similar exercise for a typical cool DA star in our sample. The results indicate that the $\log g$ solution shifts towards lower values, by roughly ~ 0.5 dex, as more lines are included in the fitting procedure. This trend occurs for all cool DA stars in our sample, and it is observed with all the model grids we have computed, no matter what atmospheric composition (i.e. mixed H/He models) or line profile theory we assumed. We believe that the results shown here represent the ultimate proof that best fitted models fail to properly match the spectroscopic data.

4. EVIDENCE FROM TRIGONOMETRIC PARALLAX MEASUREMENTS

In this section, we look at alternative methods, independent of spectroscopy, to measure the surface gravity — or equivalently the radius or the mass — of cool DA stars. The best independent method for measuring the atmospheric parameters of cool white dwarfs is the photometric technique, illustrated in the left panels of Figure 2, where optical and near-infrared photometric data are compared with the predictions of model atmospheres (see, e.g., Bergeron et al. 2001, for details). With this method, only the effective temperature and the solid angle $\pi(R/D)^2$ are considered free parameters. When the distance D is known from trigonometric parallax measurements, one directly obtains the radius R of the star, which can then be converted into mass or $\log g$ using evolutionary models. This method works

best for cool white dwarfs since the spectral energy distributions of hotter stars become less sensitive to temperature. Also, since they are generally more distant, accurate trigonometric parallaxes are more difficult to obtain.

Boudreault & Bergeron (2005) used trigonometric parallax measurements for 52 DA stars to compare the photometric masses with those obtained from the spectroscopic technique. The results (see their Fig. 1) reveal that the spectroscopic masses are in many cases larger than the photometric masses. Bergeron et al. (2007) extended this analysis by comparing photometric and spectroscopic masses for 92 DA stars. While the mean photometric mass of the sample appears slightly larger than the spectroscopic mean for hot DA stars ($M \sim 0.6 M_{\odot}$; see their Fig. 4), the dispersion of the photometric masses is significantly larger than that obtained from spectroscopy, a result that suggests a variable level of accuracy in the trigonometric parallax measurements. Bergeron et al. (2007) also compared their spectroscopic masses with those inferred from gravitational redshift measurements, although the comparison remained inconclusive because of the large uncertainties associated with the redshift velocities, which are intrinsically more difficult to obtain than any other measurement made with other techniques.

We conduct here a new comparison of photometric and spectroscopic masses, but in light view of the previous studies discussed above, we restrict our analysis to a well defined sample of homogeneous parallax measurements for which we can better account for the uncertainties. For instance, Bergeron et al. (2001, and later studies) relied on trigonometric parallaxes taken from the Yale parallax catalog (van Altena et al. 1994). However, since this catalog represents a compilation of different sources of parallax measurements, properly averaged with various weights, the adopted values may exhibit a larger dispersion than the original sources. Because it is also not clear what other corrections are used in the Yale Catalog, we decided to go back to the original measurements in order to build a more homogeneous sample. The first sample discussed here is drawn from the original USNO parallax measurements obtained from photographic plates (Harrington & Dahn 1980, and follow-up papers). This sample includes 26 DA white dwarfs with parallax uncertainties less than 12%, and for which we also have high signal-to-noise spectroscopy (from Gianninas et al. 2009) as well as optical *BVRI* and infrared *JHK* photometry (from Bergeron et al. 2001). We then compute the atmospheric parameters by using both photometric and spectroscopic techniques. For the former method, we rely on the prescription of Holberg & Bergeron (2006) to convert the magnitudes into average fluxes. The differences between spectroscopic and photometric masses (and temperatures) are displayed in Figure 11 as a function of T_{eff} (photometric); known or suspected double degenerate binaries are shown as open circles (see Table 2 of Bergeron et al. 2001). The temperatures obtained from both methods are generally in agreement, within the uncertainties, with the exception of some doubles degenerates

and the two hottest stars in our sample. For the mass comparison, no clear conclusion can be drawn for individual objects since the observed dispersion is rather large. However, if we exclude the double degenerates, the spectroscopic masses are larger than the photometric masses by $\sim 0.08 M_{\odot}$, on average, although the differences appear larger for stars above 8000 K; in fact, if we consider only stars with $T_{\text{eff}} > 8000$ K, the difference in mean mass increases to a value of $0.11 M_{\odot}$. This result can be compared to the estimated increase in mass below $T_{\text{eff}} = 12,500$ K observed in the top panel of Figure 9, which is of the order of $0.13 M_{\odot}$, a value entirely compatible with the mass difference observed in Figure 11. We must therefore conclude that the photometric masses are reasonably sound, and that the high- $\log g$ problem rests with the spectroscopic approach.

Next, we use a more recent sample drawn from the CCD parallax survey of nearby white dwarfs of Subasavage et al. (2009). This sample contains 8 DA stars for which we perform the same analysis as above, with *VRIJHK* photometry (with CTIO passbands for the *R* and *I* filters) and trigonometric parallaxes taken from Subasavage et al. The comparison of the photometric and spectroscopic parameters is displayed in Figure 12. First of all, we can see that the high accuracy of the parallax data significantly reduces the error bars. The object shown by the open circle is LHS 4040 (2351–335), for which the *JHK* photometry has the largest uncertainties in Table 3 of Subasavage et al. (2009) because of some contamination from a nearby M dwarf (LHS 4039). If we exclude this star, the mean mass difference is about $0.12 M_{\odot}$, a value comparable to that obtained from the USNO sample. We cannot help noticing, once again, that the largest temperature differences occur for the hottest stars in the sample. If we assume that the atmospheric parameters obtained from the photometric technique are reliable, it is possible to compute model spectra with these parameters and compare them with the observed optical spectra. This exercise is illustrated in the right panels of Figure 13 for the three hottest stars in the Subasavage et al. sample, while the left panels show the best fits obtained from the spectroscopic technique. This comparison allows us to evaluate how the model spectra need to be corrected to yield lower spectroscopic masses. The results suggest that the higher Balmer lines are predicted to be too sharp by the models and the lower series are predicted to be somewhat too narrow. Nevertheless, the differences in the model spectra are obviously a lot more subtle than the high-mass problem they give rise to (see Fig. 9).

There are unfortunately very few other independent verifications of $\log g$ or mass measurements that can be used below $T_{\text{eff}} = 13,000$ K. More recent USNO parallaxes with CCD observations have not been published yet, except for a very small sample (Monet et al. 1992). One very interesting result with this ongoing survey is the very massive DA star LHS 4033, for which the high mass near the Chandrasekhar limit is predicted both from the spectroscopic and the photometric methods (Dahn et al. 2004). There are also a few more recent parallax

samples, such as that of Ducourant et al. (2007), but these are mostly oriented towards very cool and faint halo white dwarfs, with very few DA stars above 7000 K. Another way to estimate masses near the ZZ Ceti instability strip is based on color indices that measure the strength of the Balmer jump, which becomes sensitive to $\log g$ in this temperature range (see, e.g., Weidemann & Koester 1984). Even then, very high precision photometry is required to measure individual masses. Koester et al. (2009) applied this technique to the large SDSS sample to compute the average photometric $\log g$ value as a function of temperature (see their Fig. 2). On average, the photometric $\log g$ values are not shown to rise significantly in the range of $16,000 \text{ K} < T_{\text{eff}} < 9000 \text{ K}$, pointing again to a problem with the spectroscopic approach.

5. ALTERNATIVE SOLUTIONS TO THE HIGH-LOG G PROBLEM

In the remainder of this paper, we explore alternative solutions to the high- $\log g$ problem in cool DA stars. Some of these solutions have already been discussed by Koester et al. (2009), but we present here some additional arguments. The first thing to realize is that with the exception of the sudden increase in $\log g$ below $T_{\text{eff}} \sim 12,500 \text{ K}$, the *dispersion* of $\log g$ values in a given range of temperatures remains nearly identical down to $T_{\text{eff}} = 8000 \text{ K}$ (see Fig. 1). Therefore, the solution we are looking for is expected to impact *all* cool DA white dwarfs in a systematic fashion. We begin by showing in panel (a) of Figure 14 the shifts in $\log g$ as a function of effective temperature required to obtain a mean mass comparable to that of hotter DA stars. These shifts have been estimated by computing, in 1000 K temperature bins, the mean $\log g$ value for the sample displayed in Figure 1. Then, to estimate the effects of each experiment (described below) on the spectroscopic determinations of T_{eff} and $\log g$, we simply fit our reference grid of model spectra with our test grid, and report the results in the various panels of Figure 14.

5.1. Hummer & Mihalas equation-of-state: Neutral Interactions

The modeling of cool and dense plasma for a non-ideal gas — mostly volume effects accounting for the finite size of the neutral particles that can lead to pressure ionization at higher densities — has always remained one of the most difficult areas in physics. Fortunately, non-ideal effects due to neutral particles are fairly unimportant for the thermodynamical structure of hydrogen-rich white dwarf atmospheres, and they only have an impact on the excited states of hydrogen. For these applications, the simple Hummer-Mihalas occupation probability model, in which the atoms are considered as hard spheres with a constant

radius, has been used in most white dwarf atmosphere codes. In this theory, the atomic states are effectively destroyed when the distance between two particles is smaller than the corresponding atomic radii. The radius of the hydrogen hard sphere is usually taken as $n^2 a_0$ where n is the principal quantum number and a_0 is the Bohr radius. This is obviously a crude approximation that does not take into account interaction potentials. Bergeron et al. (1991) found that a direct implementation of the occupation probability formalism yields $\log g$ values that are too low in the regime where non-ideal effects become dominated by neutral interactions ($T_{\text{eff}} \lesssim 8000$ K). The problem is that the higher Balmer lines are predicted too weak at normal surface gravities. Therefore, Bergeron et al. divided the hydrogen radius by a factor of two to reduce the non-ideal effects for the higher lines of the series. In view of the preceding discussion of the simple model used to describe neutral interactions, a 50% change of the effective atomic radius is not physically unrealistic.

One problem with the parameterization of the hard sphere model used by Bergeron et al. (1991) is that, since $\log g$ values are already too high for all DA stars below $T_{\text{eff}} \sim 12,500$ K, it is not clear what value of the mean surface gravity should be used to “calibrate” the hard sphere radius. In view of these uncertainties, we simply show in panel (b) of Figure 14 how the atmospheric parameters are changed if we use the original parameterization of Hummer & Mihalas (1988) where the hydrogen radius is set to its standard value ($n^2 a_0$). The effects are small at temperatures higher than $T_{\text{eff}} \sim 10,000$ K. However, if we increase the hydrogen radius even more, the atmospheric parameters become totally unrealistic at low temperatures. The conclusion, which was understood early-on (see § 2.6 of B95), is that an inaccurate treatment of the hard sphere model in the occupation probability formalism cannot be the source of the high- $\log g$ problem.

We finally note that there is another discrepancy in the Hummer-Mihalas formalism for neutral interactions, which predicts — in cool hydrogen-atmosphere white dwarfs — a largely overestimated contribution of the bound-free opacity from the Lyman edge associated with the so-called dissolved atomic levels of the hydrogen atom, or pseudocontinuum opacity (Kowalski 2006). This is partially because the theory fails to take into account the interaction potentials for the H-H and H-H₂ collisions. More realistic calculations (Kowalski & Saumon 2006) actually show that this opacity source is completely negligible in cool DA stars and should have no effect on the spectroscopic results discussed here.

5.2. Neutral Broadening

The broadening profiles of hydrogen lines in cool DA stars become increasingly dominated by neutral broadening, for which resonance broadening is the dominant source. It

has traditionally been taken into account by using broadening parameters from Ali & Griem (1965), but new theories (Barklem et al. 2000) claim that these parameters could be in error by a factor of two, although the exact numbers are still being disputed (Allard et al. 2008). In panel (c) of Figure 14, we show how the atmospheric parameters are affected when we multiply arbitrarily the resonant broadening parameter by a factor of two. Not surprisingly, the temperature range where the effect is observed is similar to that of the non-ideal gas effects due to neutral particles, shown in panel (b). Therefore, even if neutral broadening was much in error, any improvement could not account for a shift in the mean $\log g$ values at higher temperatures.

5.3. Hummer & Mihalas equation-of-state: Charged Particle Interactions

TB09 presented the first model spectra for DA stars that took into account in a consistent way the non-ideal effects described in the Hummer-Mihalas theory both in the occupation probability and line profiles calculations. The non-ideal effects due to protons are fairly well understood and we can safely say that, with the help of plasma experiments, these effects are well described to within a few percent, especially for the hydrogen Balmer lines. One matter discussed in TB09 is that the Hummer-Mihalas formalism originally used the Holtsmark distribution to describe the proton microfields. It was later upgraded with the Hooper (1968) distribution (Nayfonov et al. 1999), including the Debye shielding effect. In panel (d) of Figure 14, we show that even by using the more general and precise microfield distribution of Potekhin et al. (2002), differences in the models remain extremely small.

It must be understood, however, that the Hummer-Mihalas occupation probability formalism is based on a dipole interaction between the absorber and the protons, an approach that fails for very close collisions. Such collisions are better described with a proper account of the colliding particle potential (see TB09 for details). Proper calculations show that the non-ideal effects described in Hummer & Mihalas (1988) cannot lower the ionization potential to energies that correspond usually to transitions between the first two levels. Therefore, the bound-free pseudocontinuum opacity from the Lyman edge can be considered negligible near the $L\alpha$ region. The transition to the Hummer-Mihalas theory at lower wavelengths is still not well understood, and a sharp cutoff of the Lyman pseudocontinuum opacity longward of $L\gamma$ ($\lambda > 972.5 \text{ \AA}$) is currently used in our models. However, as seen in panel (e) of Figure 14, even if we extend our arbitrary cutoff to $L\alpha$ ($\lambda > 1216 \text{ \AA}$), the impact on the Balmer line analysis remains completely negligible.

Finally, the Hummer-Mihalas theory also takes into account non-ideal effects due to electronic collisions. These have never been included in white dwarf model atmospheres

until the work of TB09. In panel (f) of Figure 14, we show how the atmospheric parameters are changed if this additional contribution to the occupation probability is removed from *both* the line profile and equation-of-state calculations. While these non-ideal effects cannot be neglected altogether, they have little influence on the atmospheric parameters determined from spectroscopy. Our conclusion for this section is that the high- $\log g$ problem cannot be easily explained by some inaccurate treatment of non-ideal effects due to charged particles.

5.4. H^- Continuum Opacities

The dominant source of opacity in cool DA atmospheres is the bound-free and free-free H^- opacity. The main uncertainty in the calculation of the H^- opacity is the approximation used in the wave function expansions, although the current accuracy is believed to be better than 1% (John 1988). In panel (g) of Figure 14, we artificially increased the contribution of the H^- opacity in our models by 15%. The results indicate that such uncertainties would have absolutely no effect on the spectroscopic determination of the atmospheric parameters of cool DA stars.

5.5. Convective Energy Transport

We discussed in our introduction that the use of the mixing-length theory to treat the convective energy transport in white dwarf atmospheres may represent a significant source of physical uncertainty in the calculations of the atmospheric structures. It has even been considered the only viable solution to the high- $\log g$ problem by Koester et al. (2009). Using our improved model atmospheres, we proceeded in § 3 to a recalibration of the MLT free-parameter α that describes the convective efficiency. None of the discrepancies presented in this work provide any *direct* evidence that something is wrong with the MLT framework. The only circumstantial evidence is that the sudden increase in $\log g$ values below $T_{\text{eff}} \sim 12,500$ K coincide precisely with the temperature where the extent of the hydrogen convection zone becomes significant (see Fig. 5). It is also the temperature range where our models predict that a majority of the energy flux is transported by convection in the photosphere ($\tau_R = 1$). Since convective energy transport may change dramatically the temperature and pressure structures of the atmosphere, the predicted line profiles can be affected significantly since different parts of the line profiles are formed at different optical depths.

Our first objective is to evaluate the sensitivity of the high- $\log g$ problem to the current MLT models, and investigate whether there is any way to solve the problem within the theory.

We previously discussed in § 3 that the spectroscopic technique yields different solutions for T_{eff} and $\log g$ depending on the particular choice of the free parameter α . This is why we constrained the convective efficiency by relying on independent near-UV observations. If we ignore this constraint, it is possible to achieve reasonable fits in the optical using any value of α . However, B95 showed (see their Fig. 3) that the distribution of DA stars as a function of effective temperature shows unexpected gaps or clumps both in the limit of low and high convective efficiencies. This is because the hydrogen Balmer lines, which reach their maximum strength near $\sim 13,000$ K, are predicted too strong or too weak, respectively. In panel (h) of Figure 14, we show the effect of adopting a value of $\text{ML2}/\alpha = 1.5$ (instead of 0.8) in our model calculations. The surface gravities are indeed lowered in the range $13,000 > T_{\text{eff}} > 10,000$ K, but as discussed above, the distribution of DA stars now shows an important clump in temperature since the Balmer lines are predicted too weak near $T_{\text{eff}} \sim 13,000$ K (see Fig. 4 of B95), and DA stars with the strongest lines accumulate in this region.

Even with a significantly increased convective efficiency, the $\log g$ values below 10,000 K remain too high. A variation of the convective efficiency in this particular range of temperature has little effect on the predicted line profiles, and the spectroscopic determinations of $\log g$ become somewhat independent of the particular choice of the parameter α . Indeed, convection becomes increasingly adiabatic in this range of effective temperature, and thus the convective flux becomes independent of the MLT. The temperature gradient at $\tau_R = 1$, however, is still significantly different from the adiabatic gradient ($> 5\%$) in models with $T_{\text{eff}} \sim 8000$ K. Therefore, there is still room for another convection theory that could yield different temperature profiles in the range $10,000 > T_{\text{eff}} > 8000$ K. In other words, the fact that the $\log g$ values become independent of the particular choice of α does not guarantee that we converged to the correct solution. The only conclusion we can reach so far is that *within* the MLT framework, we are unable to solve the high- $\log g$ problem.

As reviewed by Fontaine & Brassard (2008, see their § 4.1), nonadiabatic calculations require a higher convective efficiency ($\alpha = 1.0$) to account for the empirical blue edge of the ZZ Ceti instability strip. Taken at face value, this conclusion implies that convection in the atmospheric layers is less efficient than in the deeper layers. From 2D hydrodynamic simulations, Ludwig et al. (1994) also concluded that the convective efficiency must increase with depth, with a value of α at $\tau_R \sim 10$ in the range of 4 to 5. In light of these findings, we performed a final test by using a variable mixing-length as a function of depth, keeping the current value at $\tau_R = 1$.⁵ The results, not shown here, reveal that the effects produced on the

⁵More specifically, we used a linear variation with depth from $\alpha = 0.8$ at $\tau_R = 1$ to $\alpha = 3.2$ at $\tau_R = 100$.

temperature structure deep in the atmosphere have absolutely no impact on the predicted spectra. Therefore, while an increase in convective efficiency with depth may affect the predictions from pulsational models, it has little effect on model spectra of cool DA stars.

It seems we may now have reached the limit of the 1D mixing-length theory, and one is naturally looking at solutions from more realistic radiation hydrodynamic calculations, such as the 2D simulations of Ludwig et al. (1994). These calculations have not been followed up, unfortunately, since 3D stellar atmospheres with radiation hydrodynamics have become more stable and accurate (Nordlund & Stein 2009). From a limited set of models representing a typical ZZ Ceti star, Ludwig et al. (1994) concluded that the mixing-length theory is roughly correct. However, since the differences between the current model spectra and the expected spectra are rather small (see the right panels of Fig. 13), this conclusion about the validity of the MLT framework should be taken with caution since the calculations of Ludwig et al. have not been confronted to real stellar spectra. A complete grid of 2D, or even 3D models should be compared with observations before reaching this conclusion. This represents the obvious next step in attempting to solve the high- $\log g$ problem.

6. CONCLUSION

The starting point of our study was the longstanding problem that spectroscopic values of $\log g$ — or masses — of DA white dwarfs cooler than $T_{\text{eff}} \lesssim 12,500$ K are significantly higher than those of hotter DA stars, a feature observed in *all spectroscopic analyses* published to date. This discrepancy limits our ability to accurately measure the atmospheric parameters of the vast majority of DA white dwarfs older than ~ 1 Gyr, and may affect the results of ZZ Ceti pulsation analyses, as well as our ability to use white dwarf stars as precise cosmochronometers or distance indicators. The first solution proposed to explain the high- $\log g$ problem has been to recognize that a mild and systematic helium contamination from convective mixing could mimic the effects of high surface gravities. In this paper, we presented high signal-to-noise, high-resolution spectroscopic observations obtained with the Keck I telescope of the region near the He I $\lambda 5877$ line for six cool DA white dwarfs. *We did not detect helium in any of our target stars.* Upper limits on the helium abundance in five of our targets allowed us to rule out the incomplete convective mixing scenario as the source of the high- $\log g$ problem. This result is in line with the conclusions of Tremblay & Bergeron (2008) that most DA white dwarfs ($\sim 85\%$) have thick hydrogen layers ($M_{\text{H}}/M_{\text{tot}} > 10^{-6}$). In view of our results, we revisited the nature of the high- $\log g$ problem and presented evidence based on photometric masses that the conundrum lies with the spectroscopic technique itself. We showed in this context that the improved Stark profiles of Tremblay & Bergeron (2009)

for the modeling of cool DA spectra did not help to solve the problem.

In our review of alternative solutions, we concluded — as Koester et al. (2009) did — that a problem with the treatment of convective energy transport, currently the mixing-length theory, is the most plausible explanation for the high- $\log g$ problem. While nothing points to a specific discrepancy with the MLT framework, the next obvious step is to compare our current atmospheric parameters for DA stars with those eventually obtained from more detailed hydrodynamic models. Only then will we be able to confirm this hypothesis.

This work was supported in part by the NSERC Canada and by the Fund FQRNT (Québec). P.B. is a Cottrell Scholar of Research Corporation for Science Advancement. Some of the data presented here were obtained at the W. M. Keck Observatory, which is operated as a scientific partnership among the California Institute of Technology, the University of California and the National Aeronautics and Space Administration. The Observatory was made possible by the generous financial support of the W. M. Keck Foundation. This research has made use of the Keck Observatory Archive (KOA), which is operated by the W. M. Keck Observatory and the NASA Exoplanet Science Institute (NExScI), under contract with the National Aeronautics and Space Administration.

REFERENCES

- Ali, A. W., & Griem, H. R. 1965, *Physical Review*, 140, 1044
- Allard, N. F., Kielkopf, J. F., Cayrel, R., & van't Veer-Menneret, C. 2008, *A&A*, 480, 581
- Barklem, P. S., Piskunov, N., & O'Mara, B. J. 2000, *A&A*, 363, 1091
- Beauchamp, A., Wesemael, F., & Bergeron, P. 1997, *ApJS*, 108, 559
- Beauchamp, A., Wesemael, F., Bergeron, P., Liebert, J., & Saffer, R. A. 1996, in *ASP Conf. Ser. Vol. 96, Hydrogen-Deficient Stars*, ed. S. Jeffery & U. Heber (San Francisco: ASP), 295
- Becklin, E. E., Farihi, J., Jura, M., Song, I., Weinberger, A. J., & Zuckerman, B. 2005, *ApJ*, 632, L119
- Bergeron, P. 1993, in *White Dwarfs: Advances in Observation and Theory*, NATO ASI Series, ed. M. A. Barstow (Dordrecht: Kluwer Academic Publishers), 267
- Bergeron, P., Gianninas, A., & Boudreault, S. 2007, in *Proc. 15th European Workshop on White Dwarfs*, eds. R. Napiwotzki & M. Burleigh (San Francisco: ASP), 372, 29
- Bergeron, P., Leggett, S. K., & Ruiz, M. T. 2001, *ApJS*, 133, 413
- Bergeron, P., Saffer, R. A., & Liebert, J. 1992, *ApJ*, 394, 228 (BSL92)
- Bergeron, P., Wesemael, F., & Fontaine, G. 1991, *ApJ*, 367, 253
- Bergeron, P., Wesemael, F., & Fontaine, G. 1992, *ApJ*, 387, 288
- Bergeron, P., Wesemael, F., Fontaine, G., & Liebert, J. 1990, *ApJ*, 351, L21
- Bergeron, P., Wesemael, F., Lamontagne, R., Fontaine, G., Saffer, R. A., & Allard, N. F. 1995, *ApJ*, 449, 258 (B95)
- Boudreault, S., & Bergeron, P. 2005, in *Proc. 14th European Workshop on White Dwarfs*, eds. D. Koester & S. Moehler (San Francisco: ASP), 334, 249
- Dahn, C. C., Bergeron, P., Liebert, J., Harris, H. C., Canzian, B., Leggett, S. K., & Boudreault, S. 2004, *ApJ*, 605, 400
- D'Antona, F., & Mazzitelli, I. 1979, *A&A*, 74, 161

- Ducourant, C., Teixeira, R., Hambly, N. C., Oppenheimer, B. R., Hawkins, M. R. S., Rapa-
port, M., Modolo, J., & Lecampion, J. F. 2007, *A&A*, 470, 387
- Farihi, J., Jura, M., & Zuckerman, B. 2009, *ApJ*, 694, 805
- Fontaine, G., & Brassard, P. 2008, *PASP*, 120, 1043
- Fontaine, G., Brassard, P., & Bergeron, P. 2001, *PASP*, 113, 409
- Gianninas, A., Bergeron, P., & Fontaine, G. 2006, *AJ*, 132, 831
- Gianninas, A., Bergeron, P., & Ruiz, M. T. 2009, *Journal of Physics Conference Series*, 172,
012021
- Gianninas, A., Dufour, P., & Bergeron, P. 2004, *ApJ*, 617, L57
- Hansen, B. M. S., et al. 2007, *ApJ*, 671, 380
- Harrington, R. S., & Dahn, C. C. 1980, *AJ*, 85, 454
- Harris, H. C., et al. 2006, *AJ*, 131, 571
- Holberg, J. B., Barstow, M. A., & Burleigh, M.R. 2003, *ApJS*, 147, 145
- Holberg, J. B., & Bergeron, P. 2006, *ApJ*, 132, 1221
- Hooper, C. F. 1968, *Physical Review*, 169, 193
- Hummer, D. G., & Mihalas, D. 1988, *ApJ*, 331, 794
- John, T. L. 1988, *A&A*, 193, 189
- Jura, M., Munro, M. P., Farihi, J., & Zuckerman, B. 2009, *ApJ*, 699, 1473
- Kepler, S.O., Kleinman, S.J., Nitta, A., Koester, D., Castanheira, B.G., Giovannini, O.,
Costa, A.F.M., & Althaus, L. 2007, *MNRAS*, 375, 1315
- Kilic, M., Thorstensen, J. R., & Koester, D. 2008, *ApJ*, 689, L45
- Koester, D. 1976, *A&A*, 52, 415
- Koester, D., Allard, N. F., & Vauclair, G. 1994, *A&A*, 291, L9
- Koester, D., Kepler, S. O., Kleinman, S. J., & Nitta, A. 2009, *Journal of Physics Conference
Series*, 172, 012006

- Koester, D., Napiwotzki, R., Voss, B., Homeier, D., & Reimers, D. 2005, *A&A*, 439, 317
- Kowalski, P. M. 2006, *ApJ*, 651, 1120
- Kowalski, P. M., & Saumon, D. 2006, *ApJ*, 651, L137
- Lajoie, C.-P., & Bergeron, P. 2007, *ApJ*, 667, 1126
- Lemke, M. 1997, *A&AS*, 122, 285
- Liebert, J., Bergeron, P., & Holberg, J. B. 2005, *ApJS*, 156, 47
- Liebert, J., & Wehrse R. 1983, *A&A*, 122, 297
- Ludwig, H.-G., Jordan, S., & Steffen, M. 1994, *A&A*, 284, 105
- Monet, D. G., Dahn, C. C., Vrba, F. J., Harris, H. C., Pier, J. R., Luginbuhl, C. B., & Ables, H. D. 1992, *AJ*, 103, 638
- Nayfonov, A., Däppen, W., Hummer, D. G., & Mihalas, D. 1999, *ApJ*, 526, 451
- Nordlund, Å., & Stein, R. F. 2009, *American Institute of Physics Conference Series*, 1171, 242
- Potekhin, A. Y., Chabrier, G., & Gilles, D. 2002, *Phys. Rev. E*, 65, 036412
- Subasavage, J. P., Jao, W.-C., Henry, T. J., Bergeron, P., Dufour, P., Ianna, P. A., Costa, E., & Méndez, R. A. 2009, *AJ*, 137, 4547
- Tremblay, P.-E., & Bergeron, P. 2008, *ApJ*, 672, 1144
- Tremblay, P.-E., & Bergeron, P. 2009, *ApJ*, 696, 1755 (TB09)
- van Altena, W. F., Lee, J. T., & Hoffleit, E. D. 1994, *The General Catalogue of Trigonometric Parallaxes* (New Haven: Yale University Observatory)
- Vauclair, G., & Reisse, C. 1977, *A&A*, 61, 415
- Vidal, C. R., Cooper, J., & Smith, E. W. 1970, *Journal of Quantitative Spectroscopy and Radiative Transfer*, 10, 1011
- Vogt, S. S., et al. 1994, *Proc. SPIE*, 2198, 362
- Weidemann, V., & Koester, D. 1984, *A&A*, 132, 195
- Zuckerman, B., Koester, D., Melis, C., Hansen, B. M., & Jura, M. 2007, *ApJ*, 671, 872

Table 1. Upper Limits on the Helium Abundance in Cool DA White Dwarfs

WD	Name	T_{eff} (K) ^a	$\log g^{\text{a}}$	He/H (3σ)	Note
0133–116	Ross 548	12470	8.05	<0.04	1
0415+271	HL Tau 76	11780	7.99	<0.11	1
1855+338	G207-9	12390	8.42	<0.09	1
1935+276	G185-32	12630	8.13	<0.04	1
2246+223	G67-23	10720	8.89	<1.42	
2326+049	G29-38	12200	8.22	<0.04	1,2

^a T_{eff} and $\log g$ assume pure hydrogen models.

Note. — (1) ZZ Ceti stars; (2) DAZ star with a circumstellar disk.

Fig. 1.— Distribution of $\log g$ as a function of effective temperature for DA white dwarfs drawn from the sample of Gianninas et al. (2009). The atmospheric parameters are determined using the reference model grid described in this work (see § 3), which is based on the improved Stark broadening profiles of TB09. Evolutionary models at constant mass from Fontaine et al. (2001) are shown with dashed lines and identified on the righthand side. The circles indicate the location of the six white dwarfs observed with HIRES on the Keck I 10-m telescope, and identified in Table 1.

Fig. 2.— Our best spectroscopic and photometric fits to the DA star LHS 3254 (1655+215) using pure hydrogen models (*top panels*). In the left panel, the error bars represent the observed fluxes derived from optical *BVRI* and infrared *JHK* magnitudes, while the corresponding model fluxes are shown as filled circles. The 0.43 dex discrepancy in $\log g$ between both fitting techniques can be resolved if helium is allowed in the atmosphere (*bottom panels*). From a qualitative point of view, both the pure hydrogen and mixed He/H solutions are indistinguishable. This is an updated version of Figure 20 from Bergeron et al. (2001).

Fig. 3.— Helium abundance determinations as a function of T_{eff} for the cool DA white dwarfs in the sample of Gianninas et al. (2009, same as Fig. 1), assuming a mass of $0.649 M_{\odot}$ for all stars. The two objects labeled in the figure are discussed in the text. The downward arrows at the bottom of the figure represent the objects for which the spectroscopic mass is already smaller than $0.649 M_{\odot}$. The dashed line indicates a systematic contamination of $\text{He}/\text{H} = 0.25$ used in our discussion.

Fig. 4.— Filled circles: same as Figure 1 but with the $\log g$ values converted into mass using the evolutionary models of Fontaine et al. (2001) with thick hydrogen layers; lines of constant mass at 0.55 and $0.70 M_{\odot}$ are shown as a reference. Open circles: mass distribution of white dwarfs below $T_{\text{eff}} = 12,500$ K obtained from model spectra that contain small traces of helium with $\text{He}/\text{H} = 0.25$. Such a mild but systematic helium contamination produces a consistent mass distribution throughout the entire temperature range displayed here.

Fig. 5.— Location of the hydrogen convection zone (*hatched region*) as a function of effective temperature in the pure hydrogen envelope of a $0.6 M_{\odot}$ DA white dwarf calculated with the $\text{ML2}/\alpha = 0.6$ version of the mixing-length theory (from G. Fontaine & P. Brassard 2006, private communication). The depth is expressed as the fractional mass above the point of interest with respect to the total mass of the star. The thick solid line corresponds to the photosphere ($\tau_R \sim 1$).

Fig. 6.— High-resolution spectra for the six white dwarfs observed with the HIRES spectrograph on the Keck I 10-m telescope. Predictions from model atmospheres with a systematic helium contamination of $\text{He}/\text{H} = 0.25$ are shown as thick solid lines. For four objects

(1855+338, 1935+276, 2246+223, and 2326+049), we also show as dotted lines the predicted spectra for an assumed mass of $0.649 M_{\odot}$ and helium abundances determined from our spectroscopic fits to low-resolution spectra (the two other objects have spectroscopic masses already lower than $0.649 M_{\odot}$). Both the observed and model spectra are shown with a 0.2 \AA resolution for clarity.

Fig. 7.— The observed HIRES spectrum of GD 362 (Zuckerman et al. 2007) from the Keck Observatory Archive. The raw data were reduced using MAKEE and calibrated to vacuum wavelength. We added the six similar exposures obtained over three different nights. The spectrum is used to constrain the He/H ratio using the best fit to the equivalent width of the line. The T_{eff} and $\log g$ values are determined from a fit to our low-resolution Balmer spectrum with mixed He/H models. The resulting atmospheric parameters are given in the figure.

Fig. 8.— Effective temperatures of ZZ Ceti stars derived from UV spectra compared with the optical determinations. Optical $\log g$ values are assumed in the determination of the UV temperatures. The size of the symbols reflects the different weights assigned to the UV spectra, as discussed in B95. The solid line indicates the locus where $T_{\text{eff}}(\text{optical}) = T_{\text{eff}}(\text{UV})$, while the dashed lines represent the $\pm 350 \text{ K}$ uncertainty allowed by the optical analysis. The results indicate that model atmospheres calculated with the $\text{ML2}/\alpha = 0.8$ parameterization of the mixing-length theory provide the best internal consistency between optical and UV temperatures.

Fig. 9.— Mass distribution as a function of T_{eff} for the DA white dwarfs in the sample of Gianninas et al. (2009). The atmospheric parameters are derived from spectroscopic fits using model spectra calculated with the Stark broadening profiles of TB09 (*top panel*) and with the Stark profiles from Lemke (1997) and the value of the critical field (β_{crit}) multiplied by factor of 2 (*bottom panel*). Lines of constant mass at 0.55 and $0.70 M_{\odot}$ are shown as a reference.

Fig. 10.— Solutions in a $T_{\text{eff}} - \log g$ diagram for a ZZ Ceti star using 2, 3, 4 and 5 lines ($\text{H}\beta$ up to $\text{H}8$) in the fitting procedure (represented by progressively thicker 1σ uncertainty ellipses from our fitting procedure). The different panels show the results for the two grids discussed in the text.

Fig. 11.— Differences between white dwarf parameters (effective temperature and mass) determined from the spectroscopic and photometric methods as a function of photometric temperatures. The *BVRIJHK* photometric data used in these determinations are taken from Bergeron et al. (2001) with trigonometric parallaxes from the USNO catalogs, while the optical spectra are from our own archive. The open circles represent suspected or known

double degenerates. The horizontal dotted lines correspond to a perfect match between spectroscopic and photometric parameters.

Fig. 12.— Same as Figure 11 but with a photometric sample drawn from the survey of Subasavage et al. (2009) with *VRIJK* photometry and accurate CCD trigonometric parallax measurements. The object represented by a circle (LHS 4040) is discussed in the text.

Fig. 13.— Left panels: Best spectroscopic fits for three DA stars from the sample of Subasavage et al. (2009); the atmospheric parameters are given in each panel. Right panels: Spectroscopic data for the same stars compared with model spectra *interpolated* at the T_{eff} and $\log g$ values obtained from the photometric method.

Fig. 14.— Panel (a) illustrates the shift in spectroscopic $\log g$ values as a function of T_{eff} required to have at each temperature a mean mass comparable to that of hotter DA stars. We assume for simplicity that the shift is the same for all values of $\log g$ at a given temperature. This panel serves as reference for the various experiments described at length in the text, and whose results are presented in the other panels. In each case, our reference model grid is fitted with a test grid, and the differences in the atmospheric parameters are reported in the figure. The changes in the models are: (b) the hydrogen radius taken as the Bohr radius in the HM88 theory, (c) the neutral broadening enhanced by a factor of two, (d) the Potekhin et al. (2002) proton microfield distribution instead of the Hooper (1968) distribution, (e) an alternative cut-off for the non-ideal gas effects in the UV at 1215 Å instead of 972 Å, (f) the neglect of non-ideal effects due to electronic collisions in the Hummer-Mihalas formalism, (g) the H^- opacity enhanced by 15%, and (h) the $\text{ML2}/\alpha = 1.5$ parameterization of the MLT.

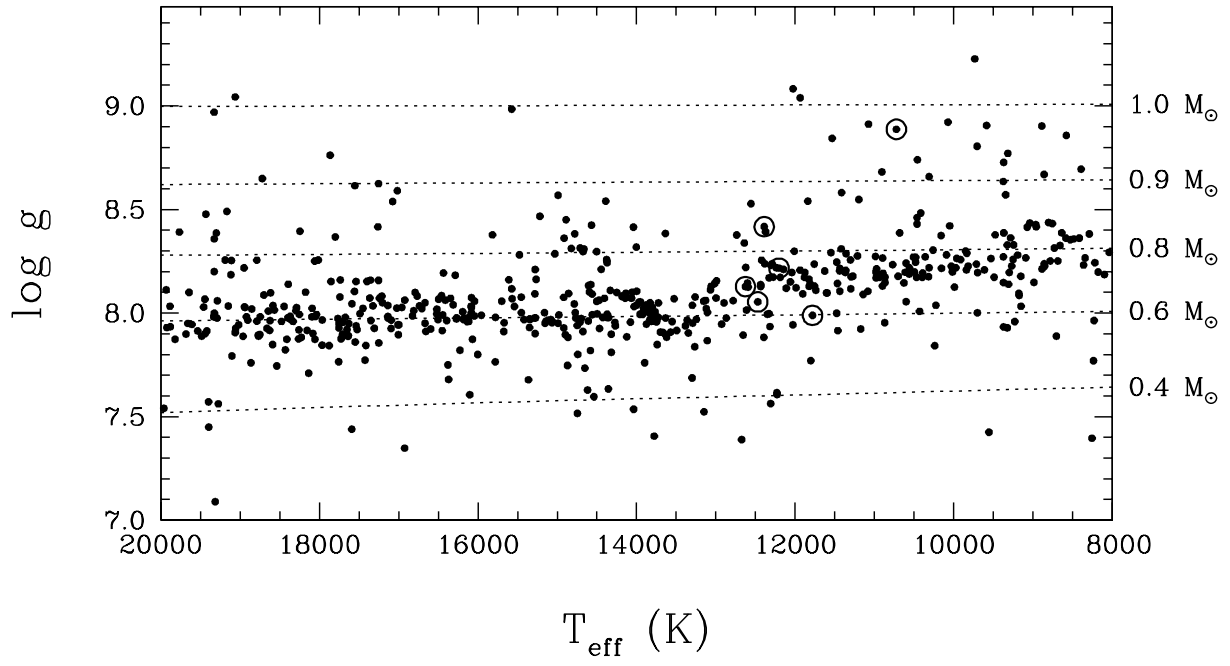


Figure 1

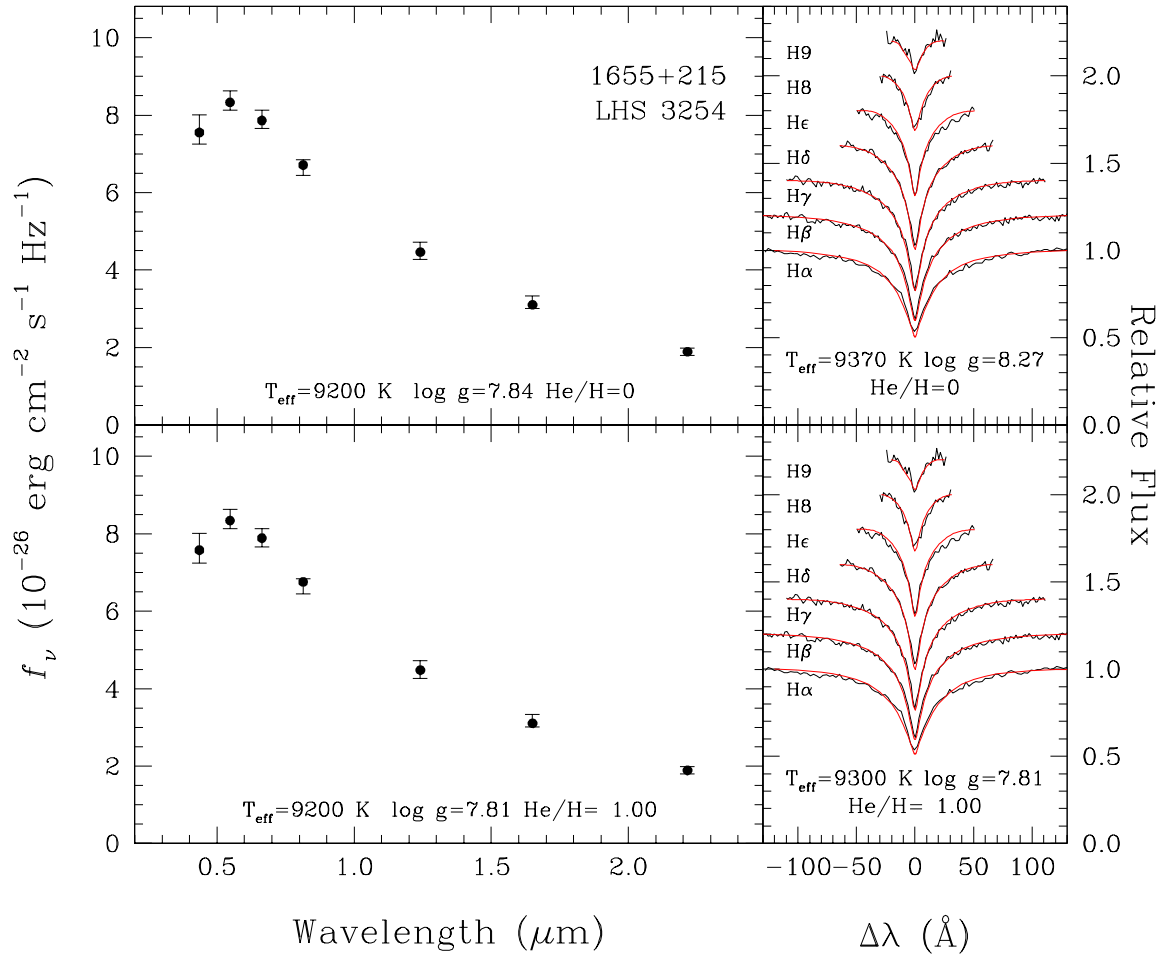


Figure 2

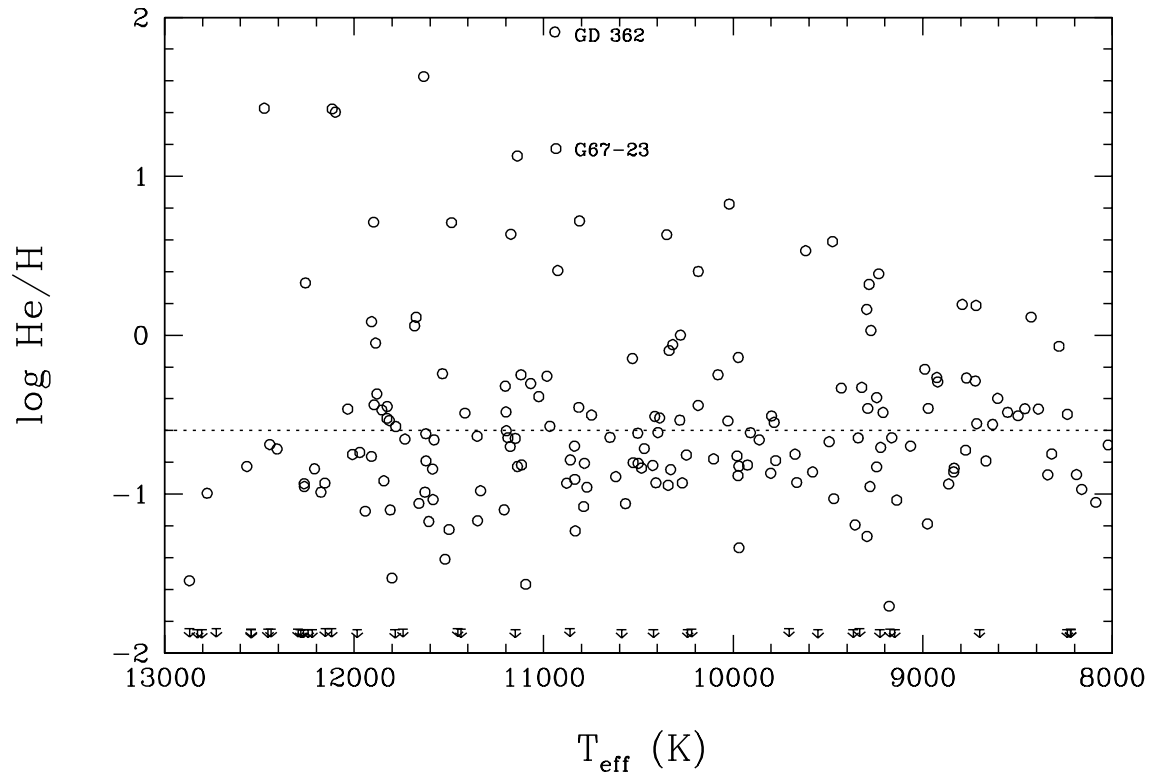


Figure 3

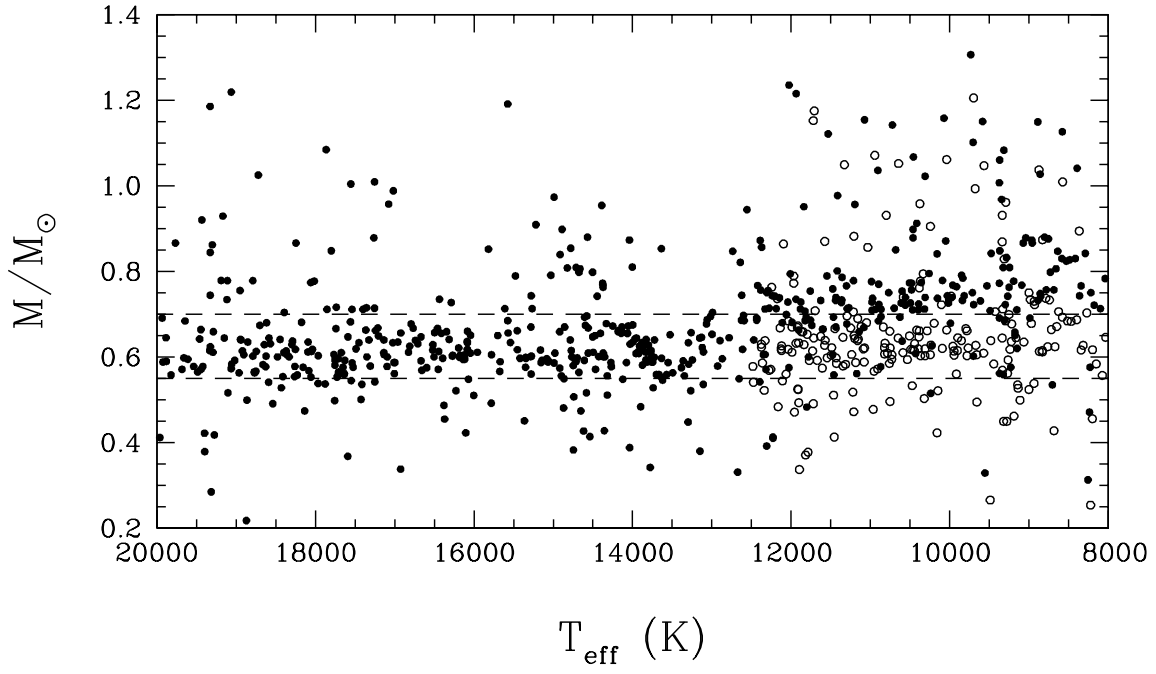


Figure 4

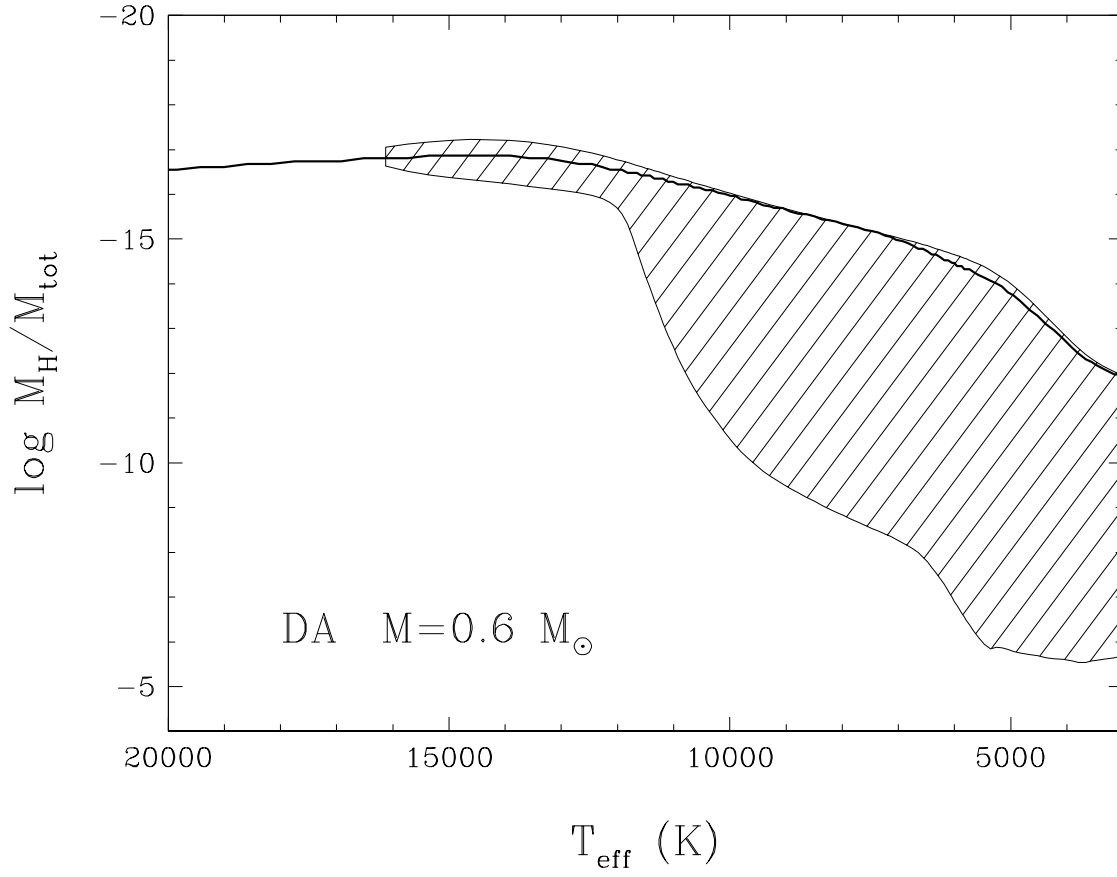


Figure 5

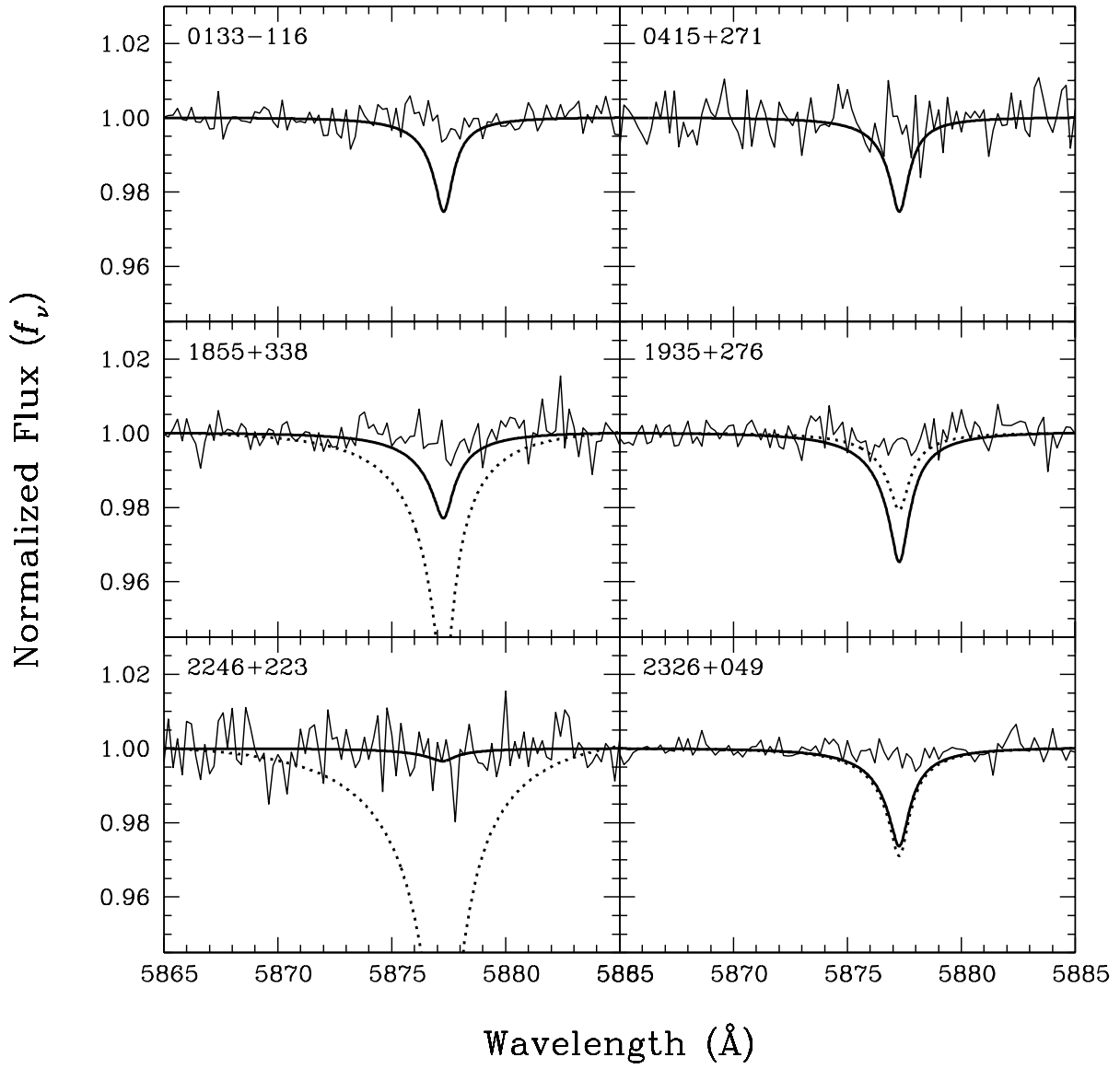


Figure 6

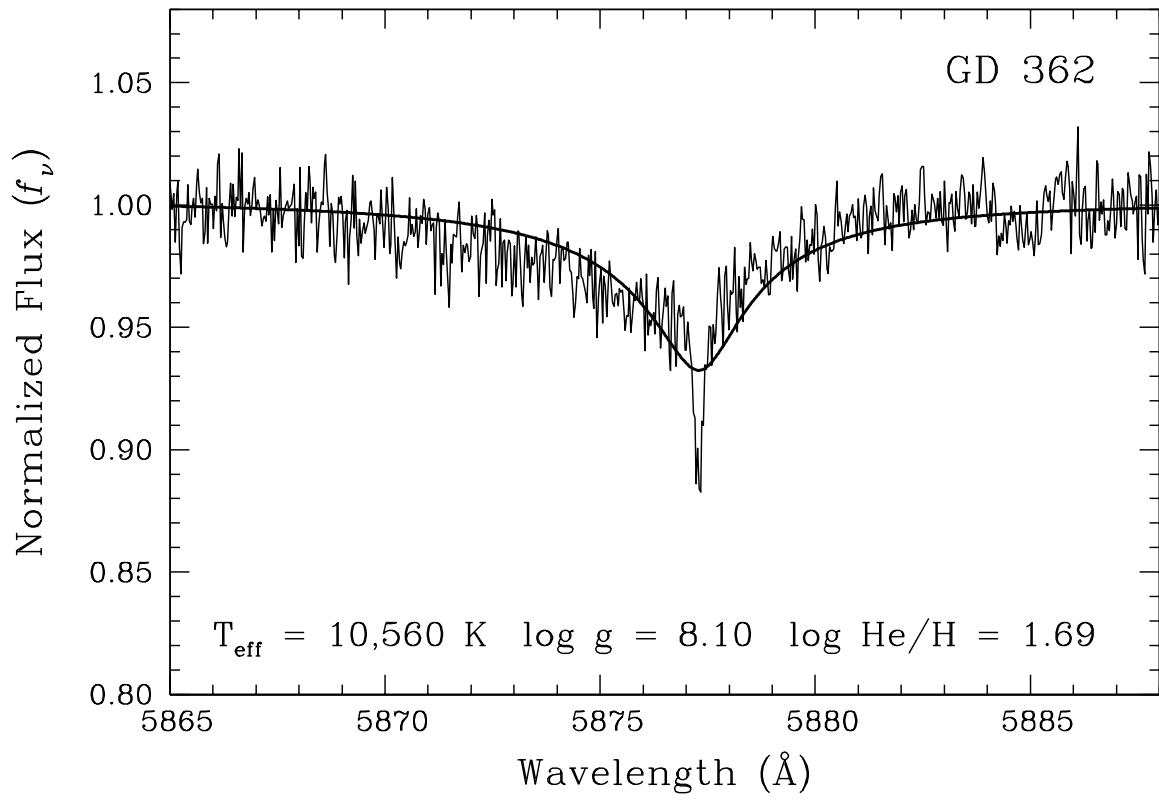


Figure 7

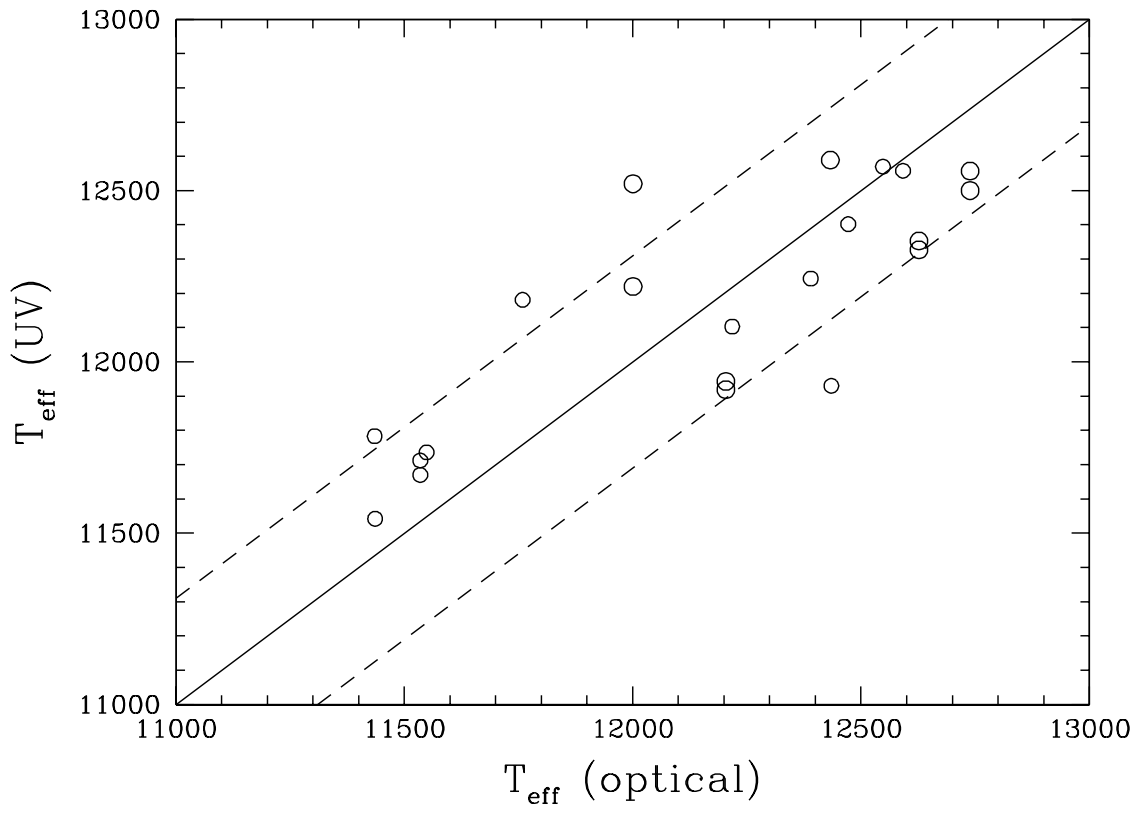


Figure 8

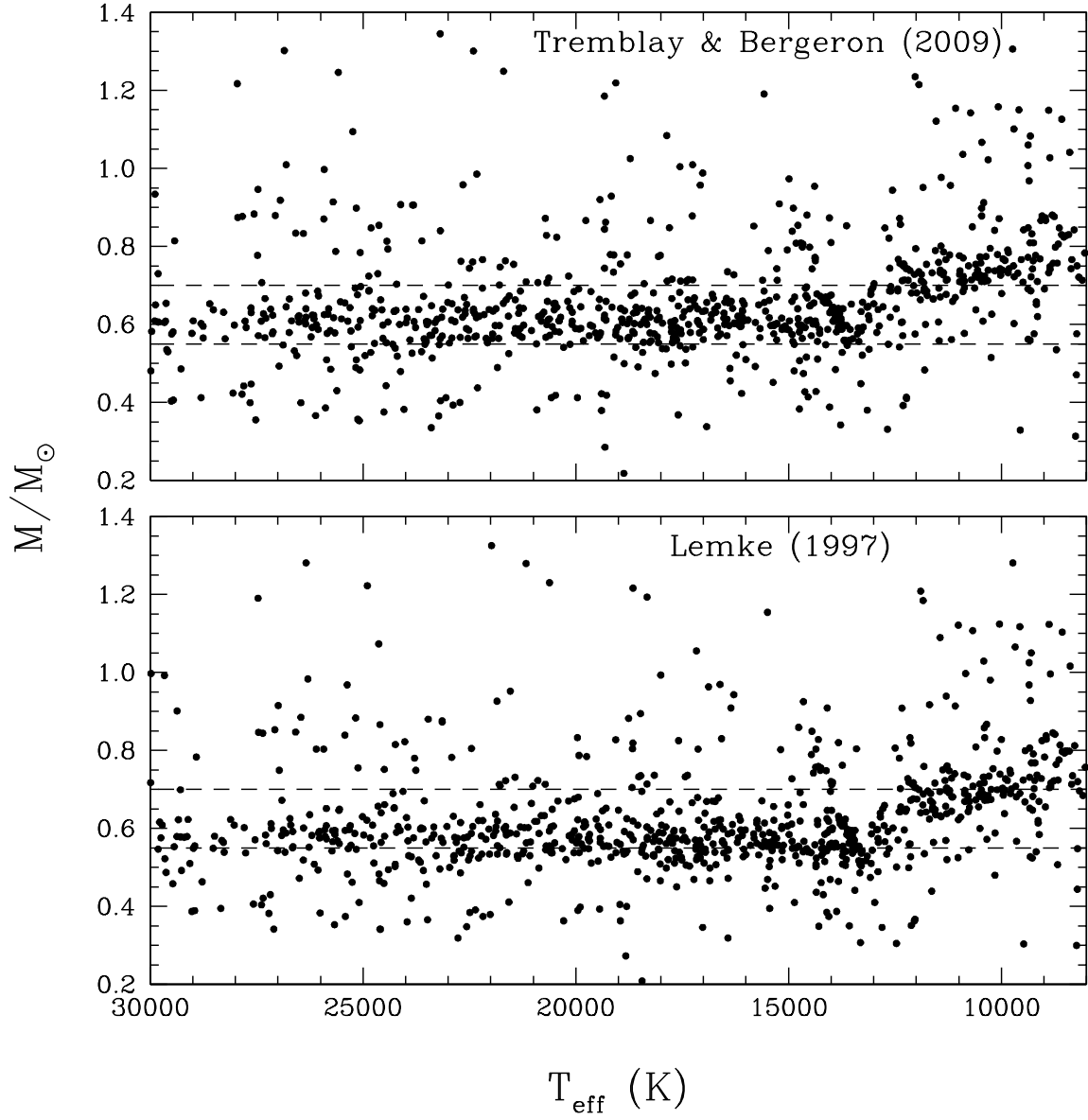


Figure 9

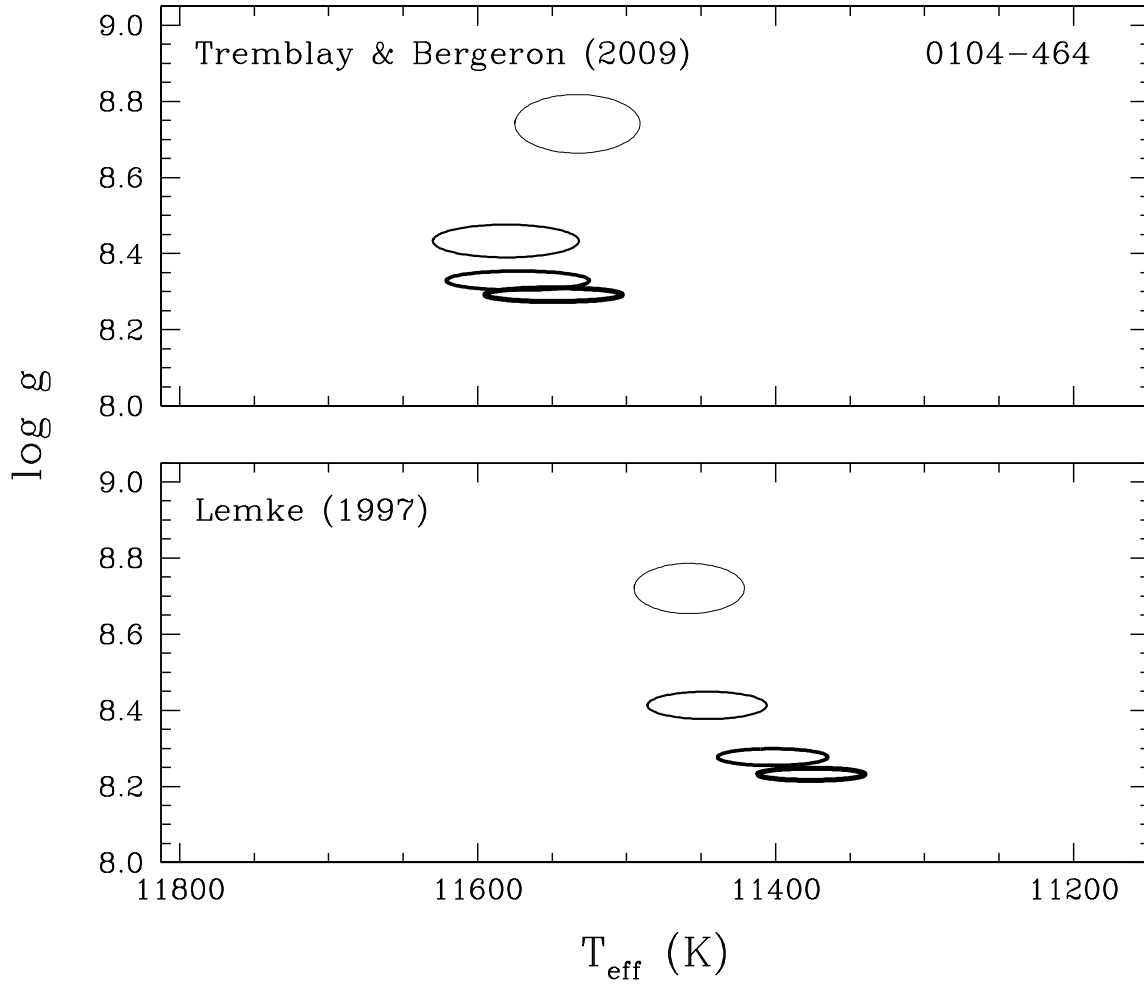


Figure 10

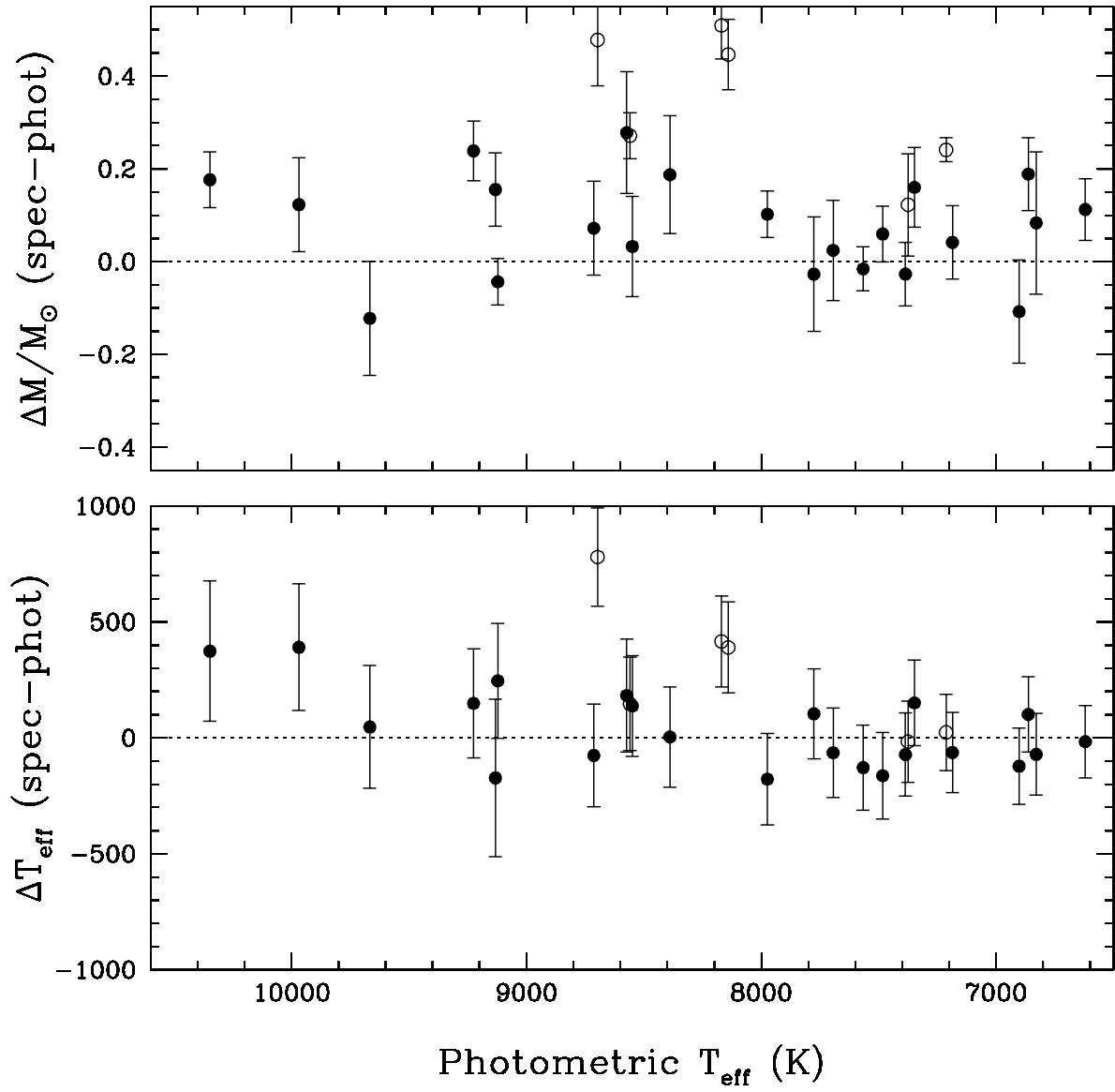


Figure 11

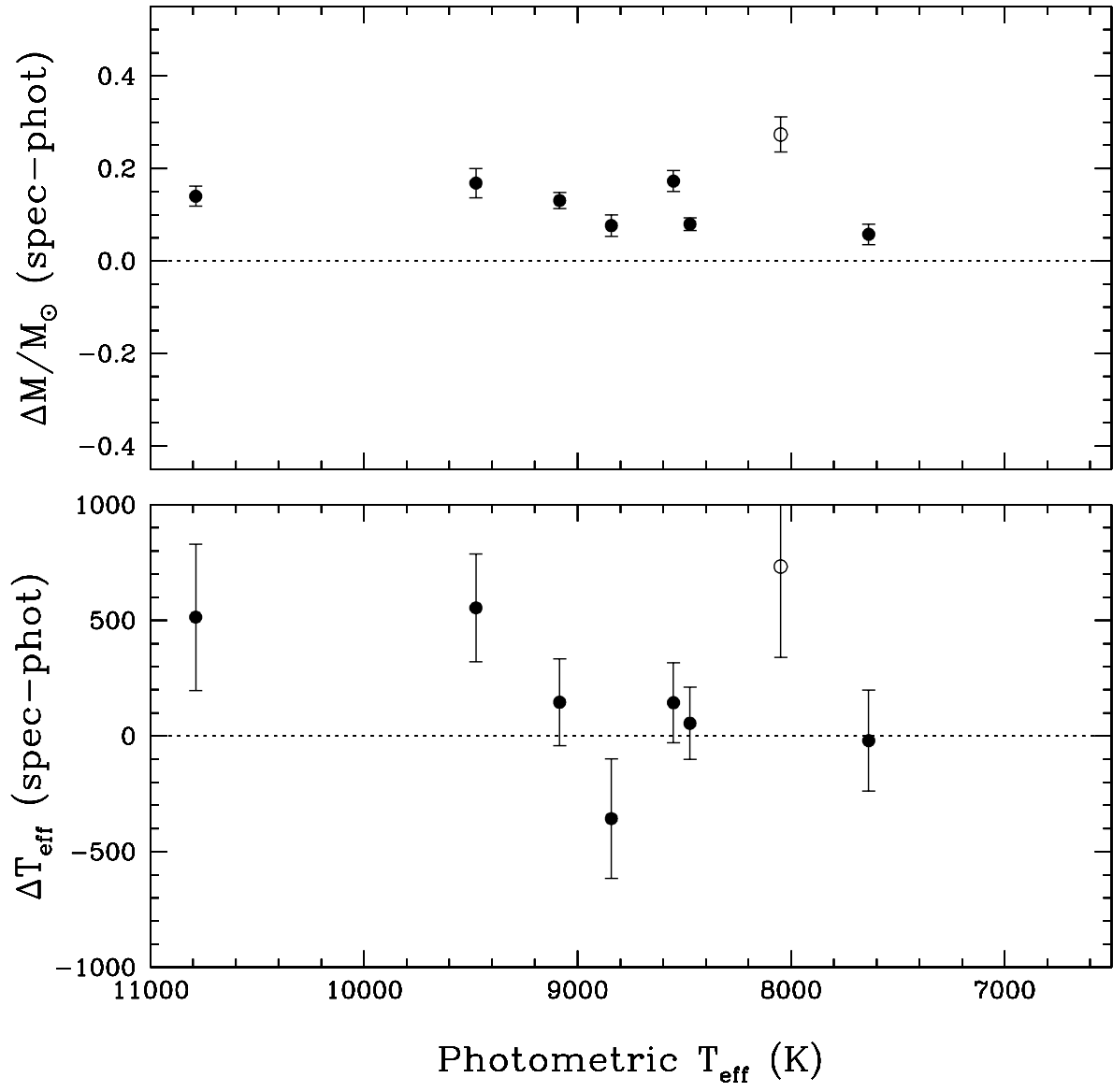


Figure 12

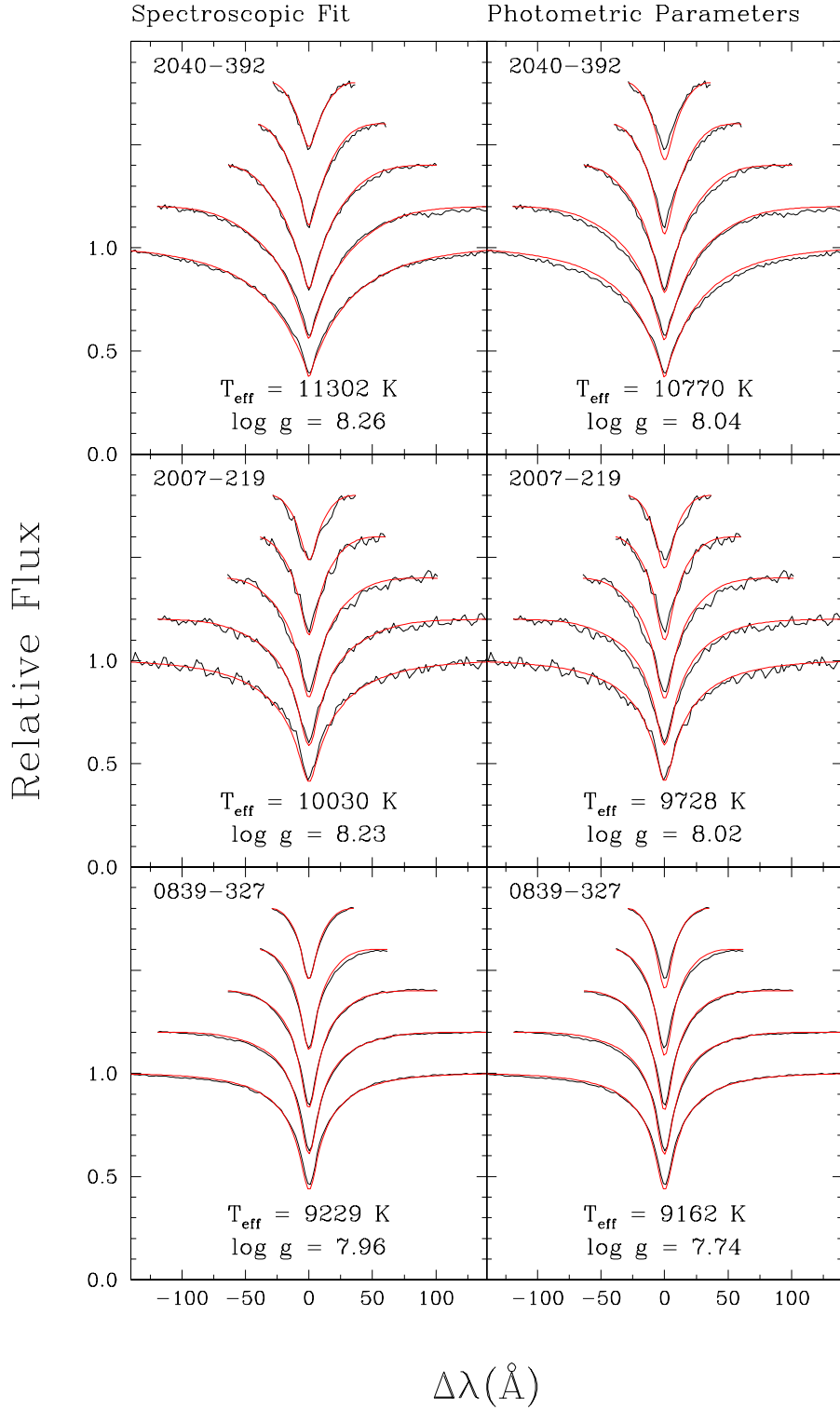


Figure 13

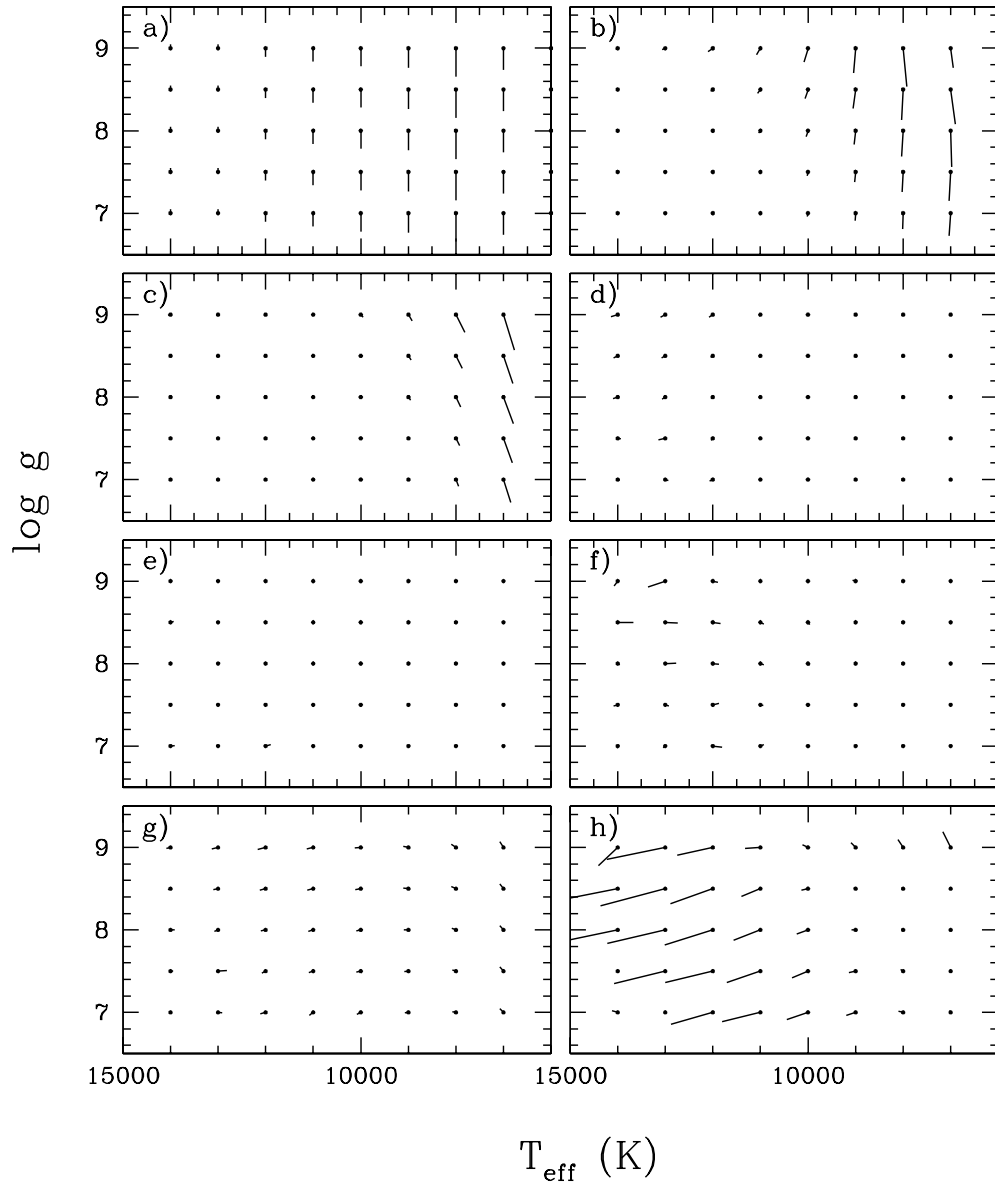


Figure 14